HHS Public Access

Author manuscript

Cell Stem Cell. Author manuscript; available in PMC 2021 May 07.

Published in final edited form as:

Cell Stem Cell. 2020 May 07; 26(5): 739–754.e8. doi:10.1016/j.stem.2020.01.020.

Hormonal suppression of stem cells inhibits symmetric cell division and gastric tumorigenesis

Wenju Chang[1,2,3,9], **Hongshan Wang**[1,3,4,9], **Woosook Kim**[3], **Yang Liu**[5], **Huan Deng**[3,6], **Haibo Liu**[3], **Zhengyu Jiang**[3], **Zhengchuan Niu**[1,3], **Weiwei Sheng**[3], **Osmel Companioni Nápoles**[3], **Yihong Sun**[1,4], **Jianmin Xu**[1,2], **Antonia Sepulveda**[7], **Yoku Hayakawa**[8], **Adam J. Bass**[5], **Timothy C. Wang**[3,10,*]

[1]Department of General Surgery, Zhongshan Hospital, Fudan University, Shanghai 200032, China

[2]Colorectal Cancer Center of Zhongshan Hospital, Fudan University, Shanghai 200032, China, Shanghai 200032, China

[3]Division of Digestive and Liver Diseases, Department of Medicine, Columbia University, College of Physicians and Surgeons, New York, NY 10032, USA

[4]Gastric Cancer Center of Zhongshan Hospital, Fudan University, Shanghai 200032, China

[5]Division of Molecular and Cellular Oncology, Dana Farber Cancer Institute, Harvard Medical School, Boston, MA 02138, USA

[6]The Fourth Affiliated Hospital of Nanchang University, Nanchang, 330003, China

[7]Department of Pathology, Columbia University, College of Physicians and Surgeons, New York, NY 10032, USA

[8]Department of Gastroenterology, Graduate School of Medicine, The University of Tokyo, Tokyo 113-0033, Japan

[9]These authors contributed equally to this work

[10]Lead contact

Summary

[*]**Correspondence:** tcw21@columbia.edu.

AUTHOR CONTRIBUTIONS

W.C. and H. W. conceptualized, designed and performed experiments, interpreted data, and wrote the manuscript. W.K performed carcinogenesis studies and isolated tumor DNA. H.L. performed LRC experiments. H.D analyzed asymmetric division in vitro. Z.J, W.H, Z.N, W.S, and O.C.N participated in lineage tracing and tumorigenesis studies. A.S contributed RNAscope studies. Y.L and A.B. analyzed exome sequencing and the mutational data. Y.S. and J.X. provided serum gastrin and G cell densities analysis. Y.H. contributed to data interpretation and manuscript writing. T.C.W. supervised the project including study design, interpretation, and writing.

Declaration of Interests

The authors declare no competing interests.

Cancer is believed to arise from stem cells, but mechanisms that limit the acquisition of mutations and tumor development have not been well-defined. We show that a +4 stem cell (SC) in the gastric antrum, marked by expression of *Cck2r (a GPCR) and* Delta-like ligand 1 (DLL1), is a label-retaining cell that undergoes predominant asymmetric cell division. This +4 antral SC is Notch1^{low}/ Numb^{+} and repressed by signaling from gastrin-expressing endocrine (G) cells. Chemical carcinogenesis of the stomach is associated with loss of G cells, increased symmetric SC division, glandular fission, and more rapid SC lineage tracing, a process that can be suppressed by exogenous gastrin treatment. This hormonal suppression was associated with a marked reduction in gastric cancer mutational load as revealed by exomic sequencing. Taken together, gastric tumorigenesis is associated with increased symmetric cell division that facilitates mutation and that can be suppressed by GPCR signaling.

Graphical Abstract

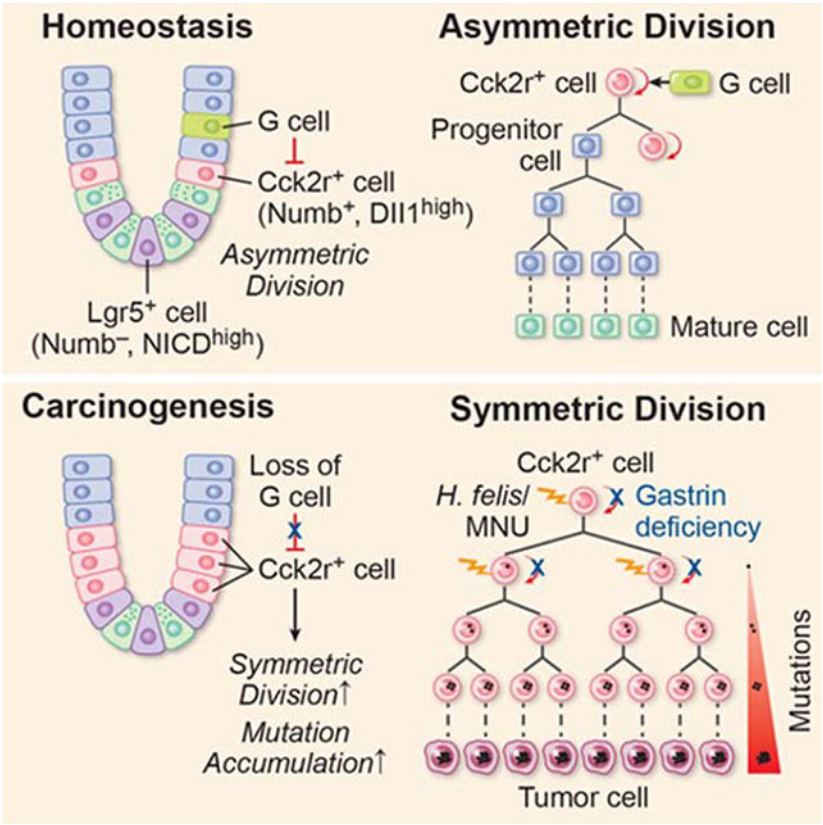

Keywords

Gastric neoplasm; carcinogenesis; stem cell; Cck2r; symmetric division; asymmetric division; gastrin; notch signaling; gene mutation

INTRODUCTION

Gastric cancer is the 5th most common malignancy and the 3rd most common cause of cancer-related death in the world (Bray et al., 2018). While the cell of origin for gastric

cancer is poorly understood, gastric stem cells are considered strong candidates given their ability to self-renew (Hayakawa et al., 2017; Reya et al., 2001).

The notion that stem cells that undergo asymmetric division (AD) are resistant to the accumulation of replication-induced mutations has been previously proposed (Cairns, 1975; Lew et al., 2008). In Drosophila, Delta-positive intestinal stem cells undergo asymmetric cell division to give rise to another stem cell and a Notch-positive progenitor (Guo and Ohlstein, 2015). However, in the mammalian gastrointestinal tract, few stem cells have been described that undergo predominant asymmetric cell division (Ohlstein and Spradling, 2007). In contrast, symmetric division (SD) gives rise to two daughter stem cells that results in an expansion of the stem cell pool, which is often required for tissue regeneration (Morrison and Kimble, 2006). In human cancers, accumulating evidence suggests that the deregulation of AD contributes to tumor initiation (Ito et al., 2010; Neumuller and Knoblich, 2009; Sugiarto et al., 2011).

Several long-lived, self-renewing stem cells have been identified in the gastric antrum (distal part of the stomach), which are characterized by unique markers such as *Lgr5* (Barker et al., 2010), *Sox2* (Arnold et al., 2011), *Axin2* (Sigal et al., 2017), *Bhlha15* (Sakitani et al., 2017), Runx1-enhancer element (Matsuo et al., 2017), and a gastrin receptor *Cck2r* (Hayakawa et al., 2015b). $Lgr5^+$ stem cells, which have been shown to serve as a cell of origin for tumors, reside at the very base of the antral glands (Barker et al., 2010; Choi et al., 2018; Demitrack et al., 2015; Li et al., 2016). A recent single cell RNA sequencing analysis revealed that antral $Lgr5^+$ cell population is heterogeneous and may include a differentiated secretory cell type (Sigal et al., 2019). In contrast, $Cck2r^+$ antral cells are largely distinct from $Lgr5^+$ stem cells and reside predominantly as single cells at the +4 position; they may represent more specifically an $Lgr5^-$ stem cell pool (Hayakawa et al., 2015b). However, while $Cck2r^+$ antral cells are bone fide antral stem cells, their regulation and role in cancer initiation have not yet been defined.

Gastrin, a peptide hormone secreted from antral gastrin-expressing endocrine cells (G cells), regulates the proximal stomach as it stimulates acid secretion and proliferation of fundic epithelial cells (Dimaline and Varro, 2014; Feng et al., 2014; Wang et al., 2000). Indeed, the gastrin/CCK2 receptor (*Cck2r)* is highly expressed in the proximal stomach, primarily in parietal cells and enterochromaffin-like (ECL) cells in the oxyntic mucosa, where gastrin's role in gastric acid physiology is well-established (Nakajima et al., 2002). Nevertheless, *Cck2r* expression is present at low levels in the gastric antrum, and $Cck2r^+$ stem cells can be activated by progastrin, a precursor form of gastrin (Hayakawa et al., 2015b). Interestingly, while progastrin promotes antral carcinogenesis, amidated gastrin (G-17) inhibits antral proliferation and gastric cancer initiation (Tomita et al., 2011), suggesting distinct roles for these related peptides. Indeed, gastrin-deficient mice develop spontaneous antral tumors (Zavros et al., 2005) and are highly susceptible to MNU-induced carcinogenesis, while hypergastrinemic mice with elevated levels of amidated gastrin are extremely resistant to antral tumorigenesis (Takaishi et al., 2009), indicating the predominant roles of amidated gastrin as a regulator of $Cck2r^+$ stem cells.

RESULTS

Antral +4 Cck2r$^+$ stem cells are DLL1$^+$ and undergo asymmetric cell division

We analyzed *Cck2r* expression in antral glands from *Cck2r*-CreERT2-BAC (Cck2r-CreERT) transgenic mice (Hayakawa et al., 2015b) crossed to *R26*-tdTomato reporter mice. Twenty-four hours after TAM induction, most of the recombined Cck2r$^+$ cells (red color) appeared as single cells (90.52±2.31%, Figure S1A, B) that overlapped well with Cck2r antibody staining (Figure 1A). These recombined Cck2r$^+$ cells accounted for 0.78±0.21% of the total glandular cell population (Figure S1C). On day 2 after TAM, many Cck2r$^+$ stem cells had undergone one cycle of cell division resulting in doublets (78.35 ± 2.84%; Figure S1D), although interestingly only one of the two cells immunostained positively with the Cck2r antibody (Figure 1A). Thus, dividing Cck2r$^+$ cells appear to give rise to both a Cck2r$^+$ cell and Cck2r$^-$ cell. By day 14, the Cck2r$^+$ cells had expanded rapidly and bi-directionally to trace whole antral gland (Figure 1A). A detailed time course and position analysis confirmed that Cck2r$^+$ cells clustered around the +4 position at early time points following TAM induction (Figure S1E). In addition, antral Cck2r$^+$ stem cells were able to give rise to all antral cellular lineages, as well as scattered corpus lineages at the antral-corpus junction (Figure S1F). We confirmed the presence of Cck2r$^+$ cells in the human gastric antrum by *in situ* hybridization (Figure S1G).

To address the relationship between Cck2r$^+$ antral stem cells and Lgr5$^+$ stem cells, we generated *Lgr5*-DTR-GFP;*Cck2r*-CreERT;*R26*-tdTomato mice. Twenty-four hours after TAM, Cck2r$^+$ cells appeared as single cells, with only ~20% overlapping with Lgr5$^+$ cells, mostly between positions +1 and +3 at the crypt base (Figure 1B). We conditionally ablated Lgr5$^+$ cells through diphtheria toxin (DT) administration as previously described (Tian et al., 2011). Complete loss of the Lgr5$^+$ cells did not perturb antral homeostasis, nor did it negatively impact Cck2r$^+$ cells tracing events (Figure 1B; S1H). Strikingly, Cck2r$^+$ cells lineage traced the antral epithelium to a greater extent following Lgr5$^+$ cell ablation, with increased Cck2r$^+$ traced cell numbers (Figure S1I) and enhanced cell division (increased Cck2r/Ki67 double positive cells) at 24h after TAM (Figure S1J, K), while the proliferation of Cck2r negative cells was unchanged (Figure S1L). Importantly, following Lgr5$^+$ cell ablation, Cck2r$^+$ cells showed stronger lineage tracing on day 7 after TAM (Figure S2A, B) and gave rise to new Lgr5-GFP$^+$ cells (yellow arrows) at the glandular base at 5 days post induction (Figure S2B, C). The number of new Lgr5-GFP$^+$ cells on day 7 after the last dose of DT treatment was similar as that of the vehicle group (Figure S2C). These data indicate that Cck2r$^+$ stem cells are fully capable of compensating for the loss of Lgr5$^+$ cells and maintaining epithelial homeostasis.

Single Cck2r$^+$ cells produce gastric spheroids that exhibit multi-potency and can survive for at least 6 months (Figure 1C). To confirm that Cck2r$^+$ cells can give rise to Lgr5$^+$ cells *in vitro*, we cultured sorted single Cck2r$^+$ cells from *Lgr5*-DTR-GFP;*Cck2r*-CreERT;*R26*-tdTomato mice after four DT injections and one day following TAM. After 3 days of culture, Lgr5-GFP$^+$ cells were found in the gastric spheroids arising from single Cck2r$^+$ cells (Figure S2D). The characteristics of sorted *Cck2r*-CreERT$^+$ cells were analyzed and compared to sorted Lgr5-GFP$^+$ cells using qPCR (Figure 1D; Table S1). Cck2r$^+$ cells showed higher

expression of *Numb* mRNA (Figure S2E). In addition, antrum tissue immunofluorescent staining also revealed that, in contrast to $Lgr5^+$ cells, $Cck2r^+$ cells were $DLL1^{high}$ and $Notch^{low}$ (Figure 1E; S2F), and only $Cck2r^+$ cells were $Numb^+$ (Figure 1F–H). Thus, *Cck2r* and *Lgr5* identified two functionally distinct antral progenitor populations. Previous studies have shown that $Lgr5^+$ cells show predominant symmetric cell division (Leushacke et al., 2013). To address the pattern of $Cck2r^+$ cells division, we immunostained for Numb protein, a Notch inhibitor and cell fate determinant that is asymmetrically partitioned during asymmetric cell division (Cicalese et al., 2009). At baseline, 79.5% of $Cck2r^+$ cells showed positive immunostaining for Numb protein (Figure 1H, I) and undergo predominantly (nearly 85%) asymmetric cell division *in vivo* (Figure 1I, J). We then used paired-cell analysis to assess *Cck2r*-CreERT-labelled cells *in vitro* (Bu et al., 2013; Bultje et al., 2009). When *Cck2r*-$CreERT^+$ cells were plated *in vitro* as single cells and allowed to progress through one cell division, co-immunofluorescence staining for Numb revealed that 18.9% of cell divisions were symmetrical (C/C), producing two $Numb^+$ daughter cells, whereas 70.9% were asymmetrical (C/D), producing one $Numb^+$ daughter and one $Numb^-$ daughter cell (Figure 2A, B), similar to the *in vivo* data.

Label retention with ^{3}H-thymidine or BrdU has been described as a property of +4 stem cells, and is rarely found in normal adult intestinal stem cells, except in response to severe DNA damage (Potten et al., 2002). Using BrdU administration and N-nitroso-methylurea (MNU) as previously described (Hayakawa et al., 2015b) to induce antral injury and stimulate $Cck2r^+$ stem cells (Figure 2C), a subset of $Cck2r^+$ stem cells were found to be $BrdU^+$ label retaining cells (LRCs; Figure 2D, E). These LRCs in the antrum were restricted to the base of the pyloric glands, and among 200 epithelial LRCs identified within a total 2000 antral glands, 3.5% of the LRCs overlapped with $Cck2r^+$ cells (Figure 2D, E).

Given that Cck2r is the primary receptor for the peptide hormone gastrin, we generated gastrin-deficient, *Cck2r*-CreERT;GAS-KO mice, and compared them to *Cck2r*-CreERT mice with normal serum gastrin levels or *Cck2r*-CreERT mice with hypergastrinemia (continuous gastrin infusion via osmotic mini-pumps, Figure 2F). GAS-KO mice showed enhanced $Cck2r^+$ cell proliferation (Figure 2G, H) and increased lineage tracing (Figure 2G, I) compared to mice with normal gastrin levels. Moreover, gastrin infusion had significant inhibitory effects on $Cck2r^+$ cell proliferation and tracing events (Figure 2G–I), although there was no change in the number of $Cck2r^+$ stem cells (Figure S2G, H). Interestingly, gastrin infusion in *Lgr5*-CreERT;*R26*-tdTomato mice showed no effect on lineage tracing, confirming that gastric $Lgr5^+$ and $Cck2r^+$ progenitors were indeed distinct (Figure 2J, K). Since the GAS-KO mouse is a whole body knockout, implying that some changes might be due to developmental defects, we investigated proliferation and tracing events in *Cck2r*-CreERT;GAS-KO mice after addition of gastrin pumps (Figure S2I). Many of the changes observed in GAS-KO mice were reversed by exogenous gastrin treatment (Figure S2J, K). Together, $Cck2r^+$ antral stem cells normally undergo asymmetric cell division, can function as LRCs, and that amidated gastrin regulates their activity.

Cck2r$^+$ stem cells are regulated by the G cell-dependent niche that is mediated by Notch signaling

The Notch signaling pathway is known to promote progenitor cell proliferation and inhibits absorptive cell differentiation in the adult intestine (Pellegrinet et al., 2011). Given that the +4 Cck2r$^+$ stem cell was Notch^{low}, we examined the effects of Notch inhibition and Notch activation on the gastric epithelium (Figure 3A; S3A, B). Notch inhibition with a gamma-secretase inhibitor (DBZ) reduced antral epithelial cell proliferation, with decrease Ki67$^+$ cells (Figure 3A; S3B). Notch inhibition also resulted in increased numbers of mucous cells (Figure S3C, D). For comparison, we studied a Notch1 gain-of-function mouse model (*Eef1a1*-LSL-*Notch1(IC)* mice) that inducibly expressed the constitutively active intracellular domain of Notch1 (NICD) (Buonamici et al., 2009). We examined the effect of Notch regulation on Lgr5$^+$ cells using *Lgr5*-CreERT mice, either alone or crossed with *Eef1a1*-LSL-*Notch1(IC)* mice. DBZ treatment caused a dramatic reduction in Lgr5$^+$ cell number, while overexpression of the NICD led to a marked increase in Lgr5+ cells (Figure 3B; S3E). In the Notch1-activated model, increased antral proliferation and decreased mucous cells were observed, as opposed to DBZ-treated animals (Figure 3A; S3B–D).

Cck2r$^+$ cell number in DBZ-treated *Cck2r*-CreERT;R26-tdTomato mice or *Cck2r*-CreERT;R26-tdTomato;*Eef1a1*-LSL-*Notch1(IC)* mice, as measured at Day 1 by FACS analysis, was not markedly altered by either Notch inhibition or NICD overexpression (Figure 3C; S3F). We analyzed tracing events in *Cck2r*-CreERT;R26-tdTomato mice and *Lgr5*-CreERT;R26-tdTomato mice on Day 7 after TAM. Decreased linage tracing events were observed after DBZ treatment from both Cck2r$^+$ (Figure 3D; S3F) and Lgr5$^+$ cells (Figure S3F–H), along with the reduction in gene expression for both *Cck2r* and *Lgr5* (Figure 3E). In contrast, overexpression of NICD resulted in increased tracing events from both populations (Figure 3D; S3H).

Given that Cck2r$^+$ cells are Notch^{low} and our earlier findings that gastrin regulates Cck2r$^+$ cell lineage tracing, we investigated whether altered Notch signaling might influence Cck2r$^+$ cells indirectly through modulation of gastrin expression. Indeed, we found that the number of gastrin$^+$ cells was increased after DBZ treatment and decreased in *Cck2r*-CreERT;*Eef1a1*-LSL-*Notch1(IC)* mice (Figure 3F, G), a finding confirmed by analysis of gastrin mRNA expression levels (Figure 3E). Next, we treated GAS-KO;*Cck2r*-CreERT;*R26*-tdTomato mice that were deficient in gastrin with DBZ (Figure 3H). While lineage tracing events were almost completely suppressed in DBZ treated *Cck2r*-CreERT;*R26*-tdTomato mice, they were partially restored in the setting of gastrin gene knockout plus DBZ treatment (Figure 3H, I), suggesting that upregulation of gastrin expression by DBZ treatment might account for the inhibitory effects of Notch inhibition on Cck2r$^+$ cell lineage tracing. We further examined the effects of Notch and gastrin by treating Cck2r-CreERT;tdTomato mice with DBZ, with or without a Cck2r antagonist, YF476. While DBZ treatment led to reduced rates of proliferation in Cck2r$^+$ cells, treatment with YF476 led to a marked increase in proliferation (Figure S3I). Thus, Notch^{low} Cck2r$^+$ stem cells appear to be regulated indirectly by Notch signaling, largely through increases in gastrin expression by neighboring G cells. However, we cannot exclude that some of the changes are due to DBZ effects on other progenitor cells.

To confirm that gastrin maintains the quiescence of Cck2r$^+$ stem cells, we examined the effects of gastrin *in vitro*. We cultured antral glands as spheroids with standard culture medium (ENR-W) plus varying concentrations of gastrin. Gastrin inhibited cell proliferation, with a visibly smaller spheroid size and a significantly decreased EdU$^+$ labeling index at the highest gastrin (100 nM) concentration (Figure 3J, K; S4A). The effects of gastrin on spheroid size could be abolished by genetic knockout of the *Cck2r* gene (*Cck2r*$^{-/-}$ mice, Figure S4B–D). On the other hand, when single Cck2r$^+$ stem cells cultured with gastrin (100 nM) and grown in soft agar, their colony formation (CFU) efficiency was significantly improved, doubling from 2.2% to 4.5%, suggesting that gastrin increases the self-renewal of Cck2r$^+$ cells (Figure 3L; S4E). After 10 days in culture, we observed a decreased size of Cck2r-derived organoids (Figure S4F) and a decreased ratio of Cck2r/Ki67 double positive cells (Figure S4G, H), suggesting that gastrin simultaneously inhibits proliferation and promotes stemness of Cck2r$^+$ cells. These gastrin-dependent changes in size, colony number (Figure 3L; S4E, F) and proliferation rate (Figure S4G, H) were abolished by treatment with YF476, a highly specific Cck2r antagonist.

Next, we investigated the effects of gastrin on the regulation of Cck2r$^+$ cells in the setting of Lgr5$^+$ cell ablation (Figure S4I), and found that gastrin decreased the rate of lineage tracing by Cck2r$^+$ cells, thus delaying the recovery of Cck2r$^+$ cell-derived Lgr5$^+$ cells (yellow color; Figure S4J). This gastrin-dependent inhibitory effect on tracing could be abolished by treatment with the Cck2r antagonist, YF476 (Figure S4J), which was consistent with the observed change in *Lgr5* gene expression (Figure S4K). Similar results were found in studies of cultured single Cck2r$^+$ cells from the *Lgr5*-DTR-GFP;*Cck2r*-CreERT;*R26*-tdTomato mice after TAM and DT treatment. Cultured Cck2r$^+$ cells were rarely if ever able to give rise to Lgr5-GFP$^+$ cells when cultured with gastrin (100nM), with more abundant Lgr5$^+$ cells produced at 3 days after gastrin was removed from the culture medium (Figure S4L). Taken together, we have identified the antral gastrin positive cell (G cell) as possibly comprising a niche cell, supporting the self-renewal ability of the +4 Cck2r$^+$ antral stem cell.

Oncogenic stress promotes symmetric cell division and stem cell expansion that is suppressed by gastrin is suppressed by gastrin

We next examined whether the Cck2r$^+$ antral stem cell could be a cell-of- origin of gastric cancer. *Cck2r*-CreERT;*R26*-tdTomato;*Apc*$^{flox/flox}$ mice. Three days after TAM and conditional *Apc* deletion in Cck2r$^+$ stem cells, single cells expressing elevated levels of the Wnt-effector protein β-catenin (black arrow) were visualized at the +4 position of the antral glands (Figure 4A). By day 7, these β-catenin$^+$ stem cells were rapidly dividing and by 4 weeks formed β-catenin-expressing adenomas that were highly proliferative (Ki67$^+$ cells; Figure 4A). Four months after TAM, the Cck2r$^+$ lineage formed macroscopic adenomas (Figure 4B), with uniform Tomato (red) expression, indicating expansion of the Cck2r$^+$ stem cell compartment (Figure 4C). Importantly, tumors specifically developed in the antrum and were never detected in the gastric corpus (Figure 4D), despite the more abundant expression of the *Cck2r*-CreERT transgene in corpus epithelial cells (Hayakawa et al., 2015b; Lee et al., 2017) (Figure 4E). As expected, a combination of *Trp53* mutation and *homozygous Apc* conditional knockout in Cck2r$^+$ antral cells led to more rapid tumor development, and generated tumors at 2 month after TAM in *Cck2r*-CreERT;*R26*-tdTomato;*Apc*$^{flox/flox}$;LSL-

Trp53R^{172H} mice (Figure 4F). Overall, while Cck2r^{+} stem cells are rarer in the antrum than most other progenitor populations, the cells appear highly susceptible to Wnt-mediated transformation.

Nevertheless, while Cck2r^{+} cells can clearly function as tumor-initiating cells after *Apc* loss, more interesting is their potential contribution in models of gastric carcinogenesis. GAS-KO mice are unusually susceptible to carcinogenesis secondary to MNU and *H. felis* infection (Tomita et al., 2011), which we postulated was due to loss of gastrin suppressive effects on Cck2r^{+} cells. We examined the effect of short-term MNU treatment on antral Cck2r^{+} cell proliferation (Figure 5A). One high-dose MNU gavage in *Cck2r*-CreERT;*R26*-tdTomato mice activated *Cck2r*$^{+}$ stem cells, with enhanced proliferation (Ki67^{+}) and more rapid tracing at 24h after MNU (Figure 5B; S5A, B). In particular, the numbers of Cck2r^{+} paired cells were increased after MNU induction, many of which were Ki67 positive (Figure 5B, C). The numbers of Cck2r^{+} paired cells in response to MNU were increased in GAS-KO mice and these increases in paired cell numbers was inhibited by gastrin infusion (Figure 5D; S5C).

Next, we examined the direct effect of MNU on symmetric versus asymmetric cell division of Cck2r^{+} stem cells. While at baseline Cck2r^{+} cells showed predominant asymmetric cell division, MNU treatment shifted their mitoses predominantly into symmetric division (Figure 5E, F). Gastrin deficiency in GAS-KO mice led to a higher frequency of symmetric division by Cck2r^{+} cells compared to WT mice at baseline, which was suppressed by gastrin infusion (Figure 5F). Furthermore, gastrin infusion was able to markedly suppress the effect of MNU on the ratio of symmetric division to asymmetric division in both WT (Figure 5F; S5D) and GAS-KO animals (Figure 5F; S5E). Interestingly, we also found that MNU treatment led to decreased G cell numbers as assessed by gastrin immunostaining (Figure S5F, G). This observation was confirmed by the finding of a marked (>50%) downregulation of antral *Gastrin* mRNA expression by qPCR (Figure S5H), suggesting that MNU can accelerates antral carcinogenesis in part through suppression of gastrin. To confirm the *in vivo* observation that gastrin and MNU treatment modulate the type of cell division by Cck2r^{+} cells, we also established an *in vitro* paired-cell assay, with analysis of Numb expression following mitosis of single Cck2r^{+} cells (Bu et al., 2013; Bultje et al., 2009). MNU-treated Cck2r^{+} paired cells had a higher frequency of symmetric division *in vitro*, and the addition of gastrin to the culture medium abolished the stimulatory effects by MNU on symmetric cell division (Figure 5G).

Finally, we examined the effects of Cck2r signaling on cell division *in vitro* by the gastric cancer cell line, AGS-E (Ai et al., 2004), which stably overexpresses the CCK receptor (Figure S5I). MTT assays indicated that gastrin (1 or 10 mmol/L) significantly suppressed the overall proliferation of Cck2r-expressing AGS-E cells but not AGS cells (as control) (Figure S5J, K). Immunofluorescence staining for Numb showed that the administration of gastrin to AGS-E cells resulted in a decreased number of Numb^{+} cells (Figure 5H) and increased the percentage of asymmetric division (Figure 5I; S5L). These data suggest that gastrin may inhibit proliferation and cancer development by reducing symmetric cell division by Cck2r^{+} cells following oncogenic stress.

Antral gastric mutagenesis and tumorigenesis are suppressed by gastrin

GAS-KO mice develop spontaneous antral tumors under conventional housing, and more rapid tumor development following MNU (Takaishi et al., 2009; Tomita et al., 2011). However, the precise role of Cck2r$^+$ antral stem cells in the development of tumors was not clarified. We administered *H. felis* and five cycles of MNU treatment to *Cck2r*-CreERT;*R26*-tdTomato mice and GAS-KO;*Cck2r*-CreERT;*R26*-tdTomato mice, and then treated them with gastrin infusion or vehicle. Mice were followed for up to 36 weeks (Figure 6A). Antral tumors were not detected either grossly or microscopically in either group at 18 weeks. However, at this time point, Cck2r$^+$ cell derived metaplastic and dysplastic foci were observed in the antrum epithelium (Figure S6A). At 36 weeks, antral tumors were observed macroscopically (Figure 6B, C), most of which showed polypoid morphology or carcinoma histology, and these lesions were strongly lineage traced from Cck2r$^+$ cells (Figure 6B; S6B). The average tumor number and tumor size were significantly greater in vehicle-treated mice compared with gastrin-treated mice, especially in vehicle-treated GAS-KO mice (Figure 6D). It is noteworthy that the vehicle-treated GAS-KO;*Cck2r*-CreERT;*R26*-tdTomato mice often developed moderately-to-poorly differentiated adenocarcinomas, whereas gastrin-treated mice did not (Figure 6E). These results indicated that hypergastrinemia suppresses the initiation and promotion stage of *H. felis*/MNU-induced antral tumors that are largely derived from Cck2r$^+$ cells.

To clarify the inhibitory mechanisms by gastrin on antral gastric carcinogenesis, we assessed proliferation as well as glandular fission, which often correlate with the expansion of gastrointestinal stem cells. We observed that gastrin deficiency increased the number of Ki67$^+$ *Cck2r*-lineage traced cells (Figure 6F; S6C), and increased the number of traced antral glands with fission (Figure 6G, H), and contiguously labeled glands in GAS-KO mice (Figure S6D). These phenotypes were all abolished by gastrin infusion (Figure S6D, E). Taken together, gastrin deficiency promoted Cck2r+ cell proliferation and Cck2r$^+$ cell-derived gland fission, which were associated with increased carcinogenesis.

To address the possible clinical relevance of these observations, we investigated gastrin$^+$ cells in antrum tissue and serum gastrin levels in patients with gastric cancer and gastritis. Using immunohistochemistry, we compared the number of gastrin$^+$ cells in the antrum of patients with a range of gastric histopathology (Figure 7A). Patients with mild (non-atrophic) gastritis had a significantly greater number of gastrin$^+$ cells compared to patients with atrophic gastritis or hyperplastic polyps, respectively (Figure 7B). Further, patients with gastric cancer showed a complete absence of gastrin$^+$ cells in antral cancer tissue, and only rare gastrin$^+$ cells in the adjacent non-tumorous antral tissue (Figure 7A, B). Finally, we found that the serum gastrin was significantly lower in patients with cancer located in the gastric antrum than in patients with corpus cancer or healthy individuals (Figure 7C). Serum gastrin level showed no correlation with tumor stage or microsatellite instability status in antrum cancer (Figure S6F, G). These results suggest that progression to antral gastric cancer correlated with decreased gastrin expression.

We hypothesized that the complete absence of gastrin, by augmenting symmetric division and enabling expansion of a stem cell population, might enable more cells to acquire additional mutations during and following MNU exposure. We collected tumor samples

from GAS-KO and WT mice that were treated with 5 cycles of MNU followed by *H. felis* infection and analyzed at 36 weeks. DNA isolated from these samples (along with matched germline DNA) were sent for exome sequencing. Importantly, we found that tumors from mice with gastrin deficiency had significantly more exome mutations (~900 on average) compared to WT mice (average <100; $P = 0.017$; Figure 7D; Table S2). The major classes of exome mutations including missense, nonsense, silent and splice site were all significantly more prevalent in the GAS-KO mice (Figure 7E; Table S3).

To evaluate this increased mutation prevalence, we first considered the possibility that the increased rate of mutations in GAS-KO mice could be attributed to a particular DNA repair defect in these mice. To address this possibility, we evaluated the mutational signatures (i.e. the pattern of specific base changes within all possible trinucleotide base contexts) to determine if any pattern related to known repair defects were present. Evaluation of the signatures relative to a benchmark set of signatures derived from human cancer genome data (Alexandrov et al., 2013), found two prominent signatures, one COSMIC signature 11, related to alkylator exposure, and COSMIC signature 26, which has associations with DNA mismatch repair. Notably, no significant enrichment in signature 26 was observed in the GAS-KO and WT mice ($P = 0.444$; Figure 7F) whereas the alkylator signature, presumably attributable to MNU exposure, was significantly enriched in the GAS-KO mice ($P = 0.030$; Figure 7G). These data suggest that the increased mutation rate with GAS-KO mice is not due to a selective DNA repair defect. Considering that more than 70% of the tumor area was derived from $Cck2r^+$ cells by linage tracing analysis (Figure 6B; Figure S6B), loss of gastrin's suppressive effects on $Cck2r^+$ cells, which was associated with an increase in symmetric division, may contribute to the accumulation of genomic mutations during tumor progression.

DISCUSSION

While intestinal stem cells marked by Lgr5 have been thoroughly investigated and validated, stem cells in other parts of the gastrointestinal tract have been less well studied. In particular, a number of distinct markers have been reported for antral gastric stem cells (Arnold et al., 2011; Barker et al., 2010; Hayakawa et al., 2015b; Matsuo et al., 2017;Sakitani et al., 2017; Sigal et al., 2017). In this study, we report distinct features and regulatory mechanism in $Cck2r^+$ antral stem cells in the setting of gastric cancer initiation. We show here that gastrin deficiency or carcinogen exposure leads to increased symmetric cell division, accumulation of mutations, and cancer progression.

While hypergastrinemia promotes gastric corpus proliferation and tumorigenesis (Hayakawa et al., 2016), gastrin deficiency has been linked to antral tumor development (Zavros et al., 2002). We have shown that gastrin deficient mice are more susceptible to MNU induced antral tumorigenesis, and that elevations in amidated gastrin suppressed antral tumorigenesis in a manner that correlated with gene silencing and epigenetic alterations of Tff1 (Takaishi et al., 2009; Tomita et al., 2011). While the specific cellular targets of gastrin's actions have remained poorly defined, we did note that Cck2r expression was present at low levels in the gastric antrum (Tomita et al., 2011). More recently, we identified Cck2r as a marker for +4 antral stem cells, and showed that progastrin was able to activate $Cck2r^+$ stem cells, and

promote gland fission and MNU carcinogenesis (Hayakawa et al., 2015b). Here, we show a direct role for amidated gastrin in regulating Cck2r$^+$ antral stem cells, and in maintaining their quiescence and asymmetric cell division. Furthermore, the current studies link Cck2r$^+$ cells more strongly to the origins of antral gastric cancer. The absence of gastrin led to increased Cck2r$^+$ stem cell proliferation and symmetric division, resulting in marked accumulation of gene mutations during antral carcinogenesis.

The current studies establish the Cck2r$^+$ antral cell as a rare but possibly dominant stem cells in the distal stomach. While Lgr5$^+$ cells were first gastric stem cells reported (Barker et al., 2010), and expand in response to *Helicobacter pylori* infection (Sigal et al., 2015), they also were shown to divide symmetrically (Leushacke et al., 2013). Furthermore, some Lgr5$^+$ cells may in fact represent differentiated secretory cells induced by increased R-spondin signaling (Sigal et al., 2019). We show here that only a minority (~20%) of Cck2r$^+$ cells are Lgr5$^+$ and only 6% of Lgr5$^+$ cells express Cck2r. In addition, while Cck2r$^+$ cells comprise a much smaller population compared to Lgr5$^+$ cells (0.74% versus 3.10% of antral epithelial cells), they lineage trace normal antral glands as well. Further, Cck2r$^+$ stem cells act as a cancer-initiating cells and tumors induced by a combination of *H. felis* infection and MNU treatment were largely (e.g. >70%) traced from Cck2r$^+$ antral stem cells. Thus, we propose that Cck2r$^+$ antral stem cells, which are mostly distinct from Lgr5$^+$ antral cells, mark more specifically an antral cancer-initiating stem cell population.

Cck2r$^+$ cells and Lgr5$^+$ cells have distinct features in their response to gastrin stimulation and Notch activation. While gastrin modulates many phenotypes in Cck2r$^+$ cells such as proliferation, cell division, and lineage tracing, it did not affect the behaviors of Lgr5$^+$ cells, demonstrating the greater relevance of Cck2r$^+$ antral stem cells to gastrin-mediated tumorigenesis. Importantly, Cck2r$^+$ cells are DLL1$^+$ while Lgr5$^+$ cells are DLL1$^-$. While Lgr5$^+$ cells in the antrum are Notch1-high and tightly regulated by Notch signaling, Cck2r$^+$ antral stem cells are Notch1-low, and thus more refractory to direct Notch manipulation. Indeed, the combination of low Notch1 expression along with strong expression of Numb, a Notch inhibitor, is thought to limit Notch1 signaling in such Numb$^+$ cells (Cicalese et al., 2009). Nevertheless, further studies are needed to define the relationship between Cck2r$^+$ and Lgr5$^+$ antral cells, and whether common stem cell properties of self-renewal and lineage tracing can be attributed to the limited overlap between the two markers.

The current data suggest that the gastrin expressing G cell in the antrum may comprises a niche cell for the +4 antral stem cell expressing Cck2r. Amidated gastrin is produced solely by G cells in the gastrin antrum, and the absence of gastrin resulted in increased Cck2r$^+$ cell proliferation and lineage tracing but overall reduced stemness (as assessed by in vitro CFU assays). In contrast, gastrin stimulation inhibited Cck2r$^+$ stem cell proliferation and tracing but increased CFU efficiency and overall stemness, likely in part through promotion of asymmetric cell division. The stem cell niche in the gut is now believed to be comprised largely by stromal cells(Hayakawa et al., 2015a), such as the recently described telocytes or myofibroblasts that provide the required Wnt and R-spondin signals (Shoshkes-Carmel et al., 2018; Sigal et al., 2017). However, as originally suggested (Sato et al., 2011), epithelial cells contribute to the niche, and this study suggests a potential role for gut endocrine cells in providing such niche signals. Indeed, the carcinogen MNU markedly reduced antral

gastrin expression, and we suggesting that downregulation of the antral gastrin niche signal may represent one mechanism by which carcinogens promote tumorigenesis. Further studies, including targeted ablation of gastrin (G) cells, will be needed to elucidate the importance of G cells in the modulation of Cck2r^{+} antral stem cells.

Asymmetric division is an evolutionarily conserved process that generates daughter cells with different fates through the unequal partitioning of fate determinants. Interestingly, our study also linked this imbalance in symmetric and asymmetric cell division to the overall process of gastric carcinogenesis. Although there is still debate about the precise roles that symmetric and asymmetric division play in tumor development, our data suggest that a shift towards symmetric cell division by Cck2r^{+} cells was associated with a striking increase in mutation rates. The difference in mutational burden was quite sizeable (~10 fold) and highly reproducible, with increases in all types of mutation. The data of course fall short of proving that symmetric cell division is directly linked to the acquisition of mutations, and further studies are needed to address this association. Asymmetric cell division by quiescent stem cells was originally proposed as a mechanism for preventing the acquisition of mutations (Cairns, 1975), but such theories have not been supported by more recent studies (Kiel MJ, 2007; Tomasetti C, 2015a). However, given that a major effect of gastrin deficiency was to increase the number Cck2r^{+} stem cells, this again points to the potential importance of stem cells as the major target for the accumulation of mutations. Indeed, recent studies suggest that given the stochastic effects of DNA replication, cancer risk is proportional to the total number of stem cell divisions, and thus the total number of stem cells (Tomasetti C, 2015b). However, while there are likely other potential explanations for the larger mutational burden in gastrin deficient mice, further studies are needed that address the relationship between aberrant asymmetric cell division and a more rapid accumulation of mutations.

STAR★METHODS

CONTACT FOR REAGENT AND RESOURCE SHARING

Further information and requests for resources and reagents should be directed to and will be fulfilled by the Lead Contact, Timothy C. Wang (tcw21@columbia.edu). All unique/stable reagents generated in this study are available from the Lead Contact with a completed Materials Transfer Agreement.

EXPERIMENTAL MODEL AND SUBJECT DETAILS

Animals—All animal studies and procedures were reviewed and approved by the Columbia University Medical Center Institutional Animal Care and Use Committee (IACUC), and all mice were bred under specific pathogen free (SPF) conditions. *Cck2r*-BAC-CreERT2-mice (Hayakawa et al., 2015b) and *Eef1a1*-LSL-*Notch1(IC)* mice (Buonamici et al., 2009) have been previously reported. LSL-*Trp53*^{R172H} mice (Renz et al., 2018) were kindly provided by Dr. Kenneth Olive (Columbia University). *Apc*$^{flox/flox}$ mice have been previously described (Westphalen et al., 2014) and were obtained from the National Cancer Institute (NCI). *Lgr5*-DTR-GFP mice, which have been previously reported (Asfaha et al., 2015), were provided by Genentech. *Lgr5*-GFP-*IRES*-CreERT2 mice (*Lgr5*-GFP mice) were provided by Dr. Hans Clevers. Gastrin-deficient (GAS-KO) mice (Koh et al., 1997) and *Cck2r*$^{-/-}$ mice (Jin et al.,

2009) have been reported in the past. *R26*-tdTomato and *Cag*-CreERT were purchased from the Jackson Laboratory. Cre recombinase was activated by oral administration of tamoxifen (2 mg/0.2 ml corn oil; Sigma-Aldrich).

Mouse gastric cancer model—Age and sex matched 8 to 12-week old mice in a C57BL/6 background were infected by oral gavage with *H. felis* in 0.2ml trypticase broth three times per week on every other day for a total dose of 100 million colony-forming units (CFU) per mouse. MNU (Gojira Fine Chemicals) was dissolved in distilled water at a concentration of 240 ppm and freshly prepared thrice per week for administration in drinking water in light-shielded bottles ad libitum. Mice were given drinking water containing 240 ppm MNU on alternate weeks for a total of 10 weeks (total exposure of 5 weeks). In the combination of *H. felis* and MNU, we administered MNU 2 weeks after *H. felis* inoculation as described previously (Hayakawa et al., 2015). Gastrin pump preparation: Gastrin (Sigma-Aldrich) was dissolved in natural saline and separated into ALZET osmotic pump (10 nmol/Kg/hour), which were set up subcutaneously for 18 weeks after first treatment with MNU.

Cell lines—The human gastric cancer cell line AGS (Sigma-Aldrich, Strains:89090402) was previously modified by stable transfection to express high levels of Cck2r (AGS-E) (Jin et al., 2013).

Human samples—Serum gastrin levels were analyzed in 46 patients with intestinal-type gastric cancer and 20 healthy patients without gastric diseases. We analyzed the serum gastrin levels based on tumor location, which included both proximal/corpus cancers (n=13) and distal/antrum cancers (n=24). The blood samples were collected on the morning before surgery while patients were still fasting. Following surgery, pathology confirmed the diagnosis of Intestinal-type gastric cancer. Blood was processed for serum, and gastrin levels were analyzed by the clinical laboratories according to standard protocols. To assess gastrin expression in patients' gastric tissues, antrum tissues were collected prospectively from patients who underwent endoscopic biopsy, including non-atrophic gastritis (n=10), atrophic gastritis (n=15), proliferative polyp (n=15), adenocarcinoma (n=10). All the tissues were stained with gastrin antibody and gastrin positive cells were calculated under arbitrarily 10 high power field of microscopy. These studies were all performed at Fudan University under an approved Human Studies IRB protocol (FDZS Y2016–0017).

METHOD DETAILS

Preparation of reagents—Gastrin (Sigma-Aldrich) was dissolved in saline and given via subcutaneous ALZET osmotic pumps (10 nmol/Kg/hour), as previously described (Chen et al., 2000). MNU (Gojira Fine Chemicals) at high dose (2400 ppm) was administered in 200 ul by oral gavage. MNU at low dose was dissolved in distilled water at a concentration of 240 ppm and freshly prepared thrice per week for administration in drinking water. Dibenzapine (DBZ, RD systems) was dissolved in 10% dimethyl sulfoxide (DMSO) and injected intraperitoneally at a dose of 20 μmol/kg for 5 days. For $Lgr5^{+}$ cell ablation in Lgr5-DTR-GFP mice, diptheria toxin (DT, Sigma-Aldrich) was administered i.p. at a dose of 20 mg/kg as previously described (Tian et al., 2011). Control groups were treated with the

appropriate vehicle or control antibodies. The Cck2r antagonist YF476 was a kind gift of Dr. Keiji Miyata and Dr. Hidenobu Yuki (Astellas Pharma, Tokyo, Japan) and has been previously reported (Lee et al., 2017) The drug was dissolved in PEG 300 at the concentration of 12 mg/mL and intraperitoneally injected twice per week at the dose of 20 mg/kg. 5-Ethynyl-2'-deoxyuridine (EdU, Life technologies) was soluble in DMSO (up to 10 mg/ml) and stored at −20°C. For in vivo cell prolif eration studies, EdU was injected by i.p. (2mg/0.2ml per 20g body weight) and mice were sacrificed and tissue collected at 2 hours post injection. BrdU was prepared with saline (2 mg/0.2 ml), and given by i.p. injection for marking label retaining cells.

Mouse treatment studies

(1) Lgr5$^+$ cell ablation: *Lgr5*-DTR-GFP; *Cck2r*-CreERT;*R26*-tdTomato mice received four dose of Diphtheria toxin (DT, 0.4 mg/20g body weight; IP) or vehicle treatment and TAM induction (2 mg/20g body weight; gavage). The first of 4 doses of DT is given at Day −6, and tamoxifen is given at day 0. Mice were killed at Day 1 for single cell sorting analysis by FACS, and for organoids culture in vitro. Mice were killed at Day 3, 5, 7 for KI67 staining, tracing event analysis, and quantification of Lgr5$^+$ cell number. Each time point had 4 mice in both group.

(2) Notch signaling regulation: Dibenzapine (DBZ, RD systems) was dissolved in 10% dimethyl sulfoxide (DMSO) and injected intraperitoneally at a dose of 20 μmol/kg for 5 days (from –Day 4 to Day 4). *Lgr5*-DTR-GFP mice, *Lgr5*-GFP-CreERT;*R26*-tdTomato mice and *Cck2r*-CreERT;*R26*-tdTomato mice were treated with DBZ or vehicle, respectively. Notch1(IC) transgenic mice (*Eef1a1-LSL-Notch1(IC)*-Cre mice) with conditional activation of NICD, which crossed with *Lgr5*-DTR-GFP mice, *Lgr5*-GFP-CreERT;*R26*-tdTomato mice and *Cck2r*-CreERT;*R26*-tdTomato mice, respectively. Mice were killed at Day 1 for quantification of cell number by FACS, and for tracing event analysis, antibody immunostaining and qPCR analysis at Day 7. Each time point had 4 mice in each group. For the quantification of proliferation of *Cck2r*-Cre$^+$cells in total *Cck2r-Cre*$^+$ cells, *Cck2r*-CreERT;*R26*-tdTomato mice were treated with Vehicle, DBZ (Five dose; 0.4 umol/20g body weight, IP) and DBZ+YF476 (0.4 mg/20g body weight, IP. Twice a week for total 3 weeks).

(3) Gastrin treatment in vivo: Gastrin (Sigma-Aldrich) was dissolved in saline and given via subcutaneous ALZET osmotic pumps (10 nmol/Kg/hour), as previously described (Chen et al., 2000). For tracing event analysis, the *Cck2r*-CreERT;*R26*-tdTomato mice and *Lgr5*-CreERT;*R26*-tdTomato mice were treated with gastrin pump for 28 days, after TAM induction, mice were killed at Day 4 and Day 6 (for Lgr5$^+$) or Day7 (for Cck2r$^+$). For in vivo cell proliferation studies, EdU was injected by i.p. (2mg/0.2ml per 20g body weight) and mice were sacrificed and tissue collected at 2 hours post injection. For gastrin effect on Lgr5$^+$ cell ablation, *Lgr5*-DTR-GFP; *Cck2r*-CreERT;*R26*-tdTomato mice received four dose of Diphtheria toxin (DT, 0.4 mg/20g body weight; IP) + vehicle, or gastrin (14 days pump) + DT treatment, or gastrin (14 days pump) + DT +YF476 (0.4 mg/20g body weight, IP. Twice a week) and TAM induction (2 mg/20g body weight; gavage). Mice were killed at Day 3, 5, 7 for KI67 staining, tracing event analysis, and quantification of Lgr5$^+$ cell number. Each time point had 4 mice in three groups.

(4) Cell division analysis in vivo: Paired cell analysis and Numb staining was done when treated with vehicle, or MNU (2400 ppm; 200 μl/ 20g body weight, gavage), or gastrin (gastrin pump, 10 nmol/Kg/hour for two weeks), or both MNU and gastrin in mice on Day 1 after TAM induction (Each group had 4 mice). The mice including *Cck2r*-CreERT;*R26*-tdTomato mice and GAS-KO/*Cck2r*-CreERT;*R26*-tdTomato mice and sacrificed at Day 1 after TAM induction, *Cck2r*-CreERT^{+}/Numb^{+} paired cells with symmetric division or asymmetric division are quantified and compared in each groups.

In vitro culture systems and treatment—Crypt and single-cell isolation and cultures were performed as described previously (Hayakawa et al., 2015b). Two or three mice were used for each experiment, and all results were confirmed by at least two independent experiments. Antrum was removed from mouse stomachs and the tissue chopped into approximately 5 mm pieces. The tissue fragments were washed with cold DPBS, and incubated in 2.5 mM EDTA in DPBS for 60 minutes on ice. The tissue fragments were suspended vigorously with a 10-ml pipette in cold DPBS containing 10% FBS, yielding supernatants enriched in crypts. Crypt fractions were centrifuged at 900 rpm for 5 minutes at 4 °C. Crypt fraction samples were passed through 70 μm filters (BD Biosciences), and centrifuged at 720 rpm for 5 minutes. Crypts were embedded in extracellular matrix (Corning) and seeded on pre-warmed 24-well or 48-well plates. After the matrix solidified, advanced DMEM/F12 medium containing penicillin/streptomycin, 50 μg/ml gentamicin, 10 mM HEPES, GlutaMAX, N2, B27 (all from Thermo Fisher Scientific), and 1 μM N-acetylcysteine (Sigma-Aldrich), 50 ng/mL EGF (Thermo Fisher Scientific), 100 ng/mL Noggin (Peprotech) and R-spondin1 was overlaid as indicated. In culture medium, 100 ng/ml Wnt3A (Peprotech) or Wnt3A-conditioned medium (1:1 concentration) was added.

Growth factors were added every other day and the entire medium was changed twice a week. Passaging of organoids was performed at day 7 as described previously (Barker et al., 2010). When passaging organoids, we dissociated organoids mechanically by 1mL tip and pipet, and replanted them. The number of organoids per well was counted on microscopic images.

Gastric single cells from antrum were isolated and cultured as described previously (Hayakawa et al., 2015b; van Es et al., 2012). Single antral stem cells were sorted from *Cck2r*-CreERT;*R26*-tdTomato mice after TAM induction, or from *Lgr5*-DTR-GFP; *Cck2r*-CreERT;*R26*-tdTomato mice after four dose of DT and TAM induction Crypts were dissociated with TrypLE express (Thermo Fisher Scientific) including 1 mg/ml DNase I (Roche) for 10 min at 37 °C. Dissociated cells were passed through a 40-μm cell strainer and washed with 2% FBS/PBS. Viable epithelial single cells were gated in FACS by forward scatter, side scatter and a pulse-width parameter, and negative staining for propidium iodide. Sorted cells were collected, pelleted and embedded in extracellular matrix, followed by seeding on a 48-well plate (50–100 cells per well). Y-27632 (10 μM, Sigma-Aldrich) was included for the first two days.

(1). For gastrin response studies, varying doses of gastrin (1nM, 10nM, 100nM) were added to the culture medium. The size and number of organoids or colony from single sorting cell were quantified under microscopy after 7–10 days' culture. The images of organoids were

acquired using fluorescent microscopy (Nikon, TE2000-U) or 2-photon microscopy (Nikon, AIP). To measure cell proliferation, Ki67 staining or 5-ethynyl-2′-deoxyuridine (EdU, 10 μM) was added to the medium of cultured cells to label cells 4 hours before fixation by 4% paraformaldehyde. (2). To examine the effects of gastrin in regulating Cck2r$^+$ cells, sorted single Cck2r$^+$ cell from *Lgr5*-DTR-GFP; *Cck2r*-CreERT;*R26*-tdTomato mice after four dose of DT and TAM induction were cultured with vehicle, gastrin 100 nM, or gastrin plus YF476 (1 μM) group. (3). To determine the effects of gastrin and MNU on Cck2r$^+$ cell division, single antral stem cells were isolated from *Cck2r*-CreERT;*R26*-tdTomato mice after treatment with vehicle, MNU (2X high dose MNU by oral gavage), or MNU (2X high dose MNU by oral gavage) + gastrin (given via Alzet pump for 7 days). Single Cck2r-tdTomato$^+$ cells were sorted from the three groups mice and then cultured in a 2D culture system with either vehicle alone (without gastrin in the culture medium), MNU (1 nM MNU in the culture medium), and MNU (1 nM) + gastrin (100 nM). (4). For colony-forming unit (CFU) efficiency from single *Cck2r*-CreERT$^+$ cell. The CFU was calculated by formed colonies/ initially seed total cells, which were treated with vehicle, gastrin (100 nM), or both gastrin and YF476 (1 uM) in the culture medium, respectively.

Lineage tracing analysis and assessment of immunofluorescence—Lineage tracing analysis of Cck2r or Lgr5 positive cells in *Cck2r*-CreERT; *R26*-tdTomato mice or *Lgr5*-GFP-*IRES*-CreERT; *R26*-tdTomato mice was performed as previously described (Barker et al., 2010). Mice were administered 2 mg tamoxifen in 200 μl corn oil by oral gavage. Following tamoxifen induction of Cre recombinase in Cck2r$^+$ or Lgr5$^+$ cells, TdTomato labelling was assessed in frozen sections at the specified time points. For in vivo experiments examining the effects of Lgr5$^+$ cell ablation, we crossed *Lgr5*-DTR-GFP mice to *Cck2r*-CreERT;*R26*-tdTomato mice. Baseline characterization of *Lgr5*-GFP$^+$ versus *Cck2r*-Cre$^+$ cells was assessed in the antral glands 24h following tamoxifen labeling of Cck2r$^+$ cells. To assess the effects of Lgr5$^+$ cell ablation, diphtheria toxin (DT; 20 mg/kg.) was administered i.p. every two days for totally 4 doses. On the last day of intraperitoneal DT injection, a single dose of tamoxifen (2 mg p.o.) was also administered to label Cck2r$^+$ stem cells. Twenty-four hours following tamoxifen and the last dose of DT, Lgr5$^+$ cell ablation and Cck2r$^+$ stem cell lineage tracing of the antrum were assessed using fluorescence microscopy Efficiency of lineage tracing was determined by quantification of the number of Cck2r$^+$ lineage traced glands per 100 crypts counted.

Paired-cell analysis—Paired-cell analysis was performed as described (Bu et al., 2013; Bultje et al., 2009). In brief, *Cck2r*-Cre$^+$ cells were plated as single cells and allowed to progress through one cell division; co-immunofluorescence staining for Numb antibody was done. *Cck2r*-Cre$^+$ cells were isolated by FACS from *Cck2r*-CreERT;*R26*-tdTomato mice at 24h after TAM induction. A single-cell suspension was resuspended in a culture medium containing DMEM/F12, 10 mM HEPES, GlutaMAX, N2, B27 (all from Thermo Fisher Scientific), and 1 μM N-acetylcysteine (Sigma-Aldrich), 50 ng/mL EGF (Peprotech), 50 ng/mL FGF (Peprotech), 100 ng/mL Noggin (Peprotech) and R-spondin1, 100 ng/ml Wnt3A (Peprotech), 7.5 μM Y-27632 and 1 μM A83–01(Sigma-Aldrich) and plated onto coverslips coated with poly-L-lysine (Sigma-Aldrich) in 24-well plates at clonal density. The cultures were maintained in a humidified incubator at 37 °C with constant 5% CO_2 supply.

Approximately 24 hours later, the cultures were fixed and immunostained with a Numb antibody (1:200). Images were acquired on an inverted epifluorescence microscope (Nikon, TE2000-U) or 2-photon microscopy (Nikon, A1P).

Label-Retaining Cell (LRC) Assay—Label retaining cells were analyzed in 12 weeks old *Cck2r*-CreERT; *R26*-tdTomato mice treated with once daily gavage of 2400 ppm MNU for two consecutive days. 5-Bromo-2'-deoxyuridine (BrdU; Sigma-Aldrich) at a dose of 2mg/0.2ml per injection was given every 8 hours for the first 72 hours post first MNU induction. The animals were then followed untreated for a period of 14 days, at which time they were given 4 mg tamoxifen induction for 24 hours and then sacrificed. BrdU labeled cells were then detected by immunofluorescence, using antibodies to BrdU (1:200, Abcam). Primary antibodies were incubated overnight, and sections subsequently were incubated with Alexa Fluor 488 secondary antibodies (Thermo Fisher Scientific) and counterstained with 4', 6-diamidino-2-phenylindole (DAPI; BD Pharmingen).

In Situ Hybridization—The Homo sapiens cholecystokinin B receptor (CCKBR) RNAscope Probe-Hs-CCKBR (Cat No. 311101, ACD bio, Abingdon, UK) was used with the Manual Assay RNAscope platform. Five-micron thick sections from FFPE blocks were hybridized and stained in the Leica Bond-III IHC and ISH automated stainer following the manufacturer instructions. The universal negative control with probes targeting the DapB gene (accession # EF191515) from the Bacillus subtilis strain SM were used in parallel (ACD bio, Abingdon, UK).

Proliferation of AGS cells and AGS-E cells—We harvested synchronized AGS-E cells using the shake-off method and plated 1×10^4 cells in chamber slides for 12 h followed by the administration of graded levels of amidated gastrin (Sigma-Aldrich) for 24 h (Schorl and Sedivy, 2007). The original parent AGS cells were employed as controls to exclude nonspecific effects of amidated gastrin. Following short-term culture, cells were stained with Numb antibody (Abcam, ab14140, 8 μg/ml) to evaluate levels of asymmetric and symmetric division of AGS-E cells. The $Numb^+$-to-$DAPI^+$ ratio was used to calculate the percentage of symmetric and asymmetric cell division by stimulated and unstimulated AGS-E cells. The symmetric division pair was defined as daughter cells which were both positive for Numb, while asymmetric cell division was defined as only 1 $Numb^+$ daughter cell. We calculated the percentage of asymmetric division pairs in the total cellular pool.

Tissue collection and histological analysis—Following isoflurane inhalation, blood was immediately collected into serum collection vials (BD Biosciences) by incision of the brachial artery or vein, and mice were then euthanized by cervical dislocation. The stomach and proximal duodenum were removed and the stomach incised along the greater curvature. Linear gastric strips from the lesser curvature were fixed overnight in 10% phosphate-buffered formalin or 4% paraformaldehyde, embedded into paraffin block or OCT compounds. Histological scoring was performed according to published criteria by a board certified veterinary pathologist (S.M.) blinded to sample identity. A dysplasia score of 3.0 was considered carcinoma in situ or low-grade gastrointestinal intraepithelial neoplasia

(GIN), and a score of 4.0 represented invasive gastric cancer. The remainder of the gastric tissue was snap-frozen in dry ice and stored at −80 °C for mRN A analysis.

Quantitative analysis of mRNA expression—For the *Cck2r*, *Lgr5*, *Notch1*, *Dll1*, *Sox2*, *Axin2*, *Ascl2* and *Numb* mRNA expression analysis from sorted *Cck2r*-CreERT^{+} cells and sorted Lgr5-GFP^{+} cells, the gastric single cells from antrum were isolated as described previously (Hayakawa et al., 2015b; van Es et al., 2012). Single antral stem cells were sorted from *Cck2r*-CreERT;*R26*-tdTomato mice at 24 hours after TAM induction, or from *Lgr5*-DTR-GFP mice. All primer sequences were listed in Table S1.

For the *Cck2r*, *Lgr5*, *Notch*1, *Dll1* and *Gastrin* mRNA expression analysis from gastric antral tisuue, the longitudinal strips of gastric tissue from the anterior wall as well as the posterior wall were harvested and snap-frozen in dry ice and kept in a −80 °C freezer until processed for analysis. Total RNA was extracted with Nucleospin RNA II kit (Clontech) and cDNA was synthesized by Superscript III First-strand Synthesis System for RT-PCR (Thermo Fisher Scientific). Expression levels of indicated genes were quantified by Real-Time PCR (qPCR) assays using SYBR Green and 7300 Real Time PCR System. Primer sequences used in this experiment are available upon request.

Immunohistochemistry and Immunofluorescence—Tissues were fixed in 10% formalin or 4% paraformaldehyde overnight, embedded in paraffin, and processed by standard histological methods. Immunohistochemical staining was performed with avidin-biotin-peroxidase complex kits (Vector Laboratories, CA) according to the manufacturer's instructions. The following primary antibodies were used: anti-Ki67 (1:100, rabbit polyclonal, Abcam), anti-TFF2 antibody (1:200, Santa Cruz), anti-BrdU antibody (1:200, rat monoclonal, Abcam), anti-H/K-ATPase antibody (1:1000, mouse monoclonal, Santa Cruz), anti-Chromogranin A antibody (1:200, rabbit polyclonal, Abcam), anti-Mucin5AC antibody (1:200, goat polyclonal, Santa Cruz), anti-intrinsic factor antibody (1:200, rabbit polyclonal, Abcam), anti-gastrin antibody (1:200, rabbit polyclonal, Santa Cruz), anti-somatostatin antibody (1:200, Abcam), anti-E-cadherin antibody (1:200, Cell Signaling Technology), anti-β-catenin (1:500, mouse monoclonal, BD Bioscience), anti-DLL1 (1:200, rabbit polyclonal, Abcam), anti-activated Notch1 (1:200, rabbit polyclonal, Abcam), anti-Numb (1:200, rabbit polyclonal, Abcam), anti-β-Catenin (BD Bioscience) and anti-GFP antibody (1:200, Abcam). Primary antibodies were incubated at room temperature for one hour or at 4 °C overnig ht, in a humidified chamber. Subsequently, the sections were incubated with biotinylated secondary antibodies (Vectastain ABC kit; Vector Laboratories, Burlingame, CA) for 30 minutes, followed by incubation with avidin-coupled peroxidase (Vector Laboratories) for 30 minutes. Diaminobenzidine (DAB; Dako) as the chromogen and slides were counterstained with Mayer's hematoxylin. For immunofluorescence, Alexa Fluor 488, 594 or 647 secondary antibodies (Thermo Fisher Scientific) were used and then counterstained with 4', 6-diamidino-2-phenylindole (Vector Laboratories). EdU staining was done follow the manual instruction of the kit (Life Technologies). The number of Ki67^{+}, EdU^{+}, or *Cck2r*-cre positive cells in the stomach glands was measured at 20 different locations in the each of three group mice under the Nikon TE2000 microscope (Nikon Inc.,

Melville, NY). All values were expressed as mean ± SD (standard deviation). * $P < 0.05$, ** $P < 0.01$, *** $P < 0.001$.

Whole exome sequencing—Gastrin-deficient (GAS-KO) mice and WT mice on the C57BL/6J background were infected with *Helicobacter felis* at 6–8 weeks of age and received 5 cycles of 240 ppm MNU in drinking water for a week every other week. At 36 weeks post-MNU, antral tumor tissues and corresponding non-tumor tissues as a control for detection of mutations were collected and genomic DNA was extracted using NucleoSpin tissue kit (Macherey-Nagel) according to the manufacturer's instructions. The samples were quantified using Qubit, quality checked by gel electrophoresis, and subjected to whole exome sequencing at the Broad Institute, Columbia University Medical Center and Beijing Genomic Institute (BGI). Pair-end (PE) libraries were prepared and sequenced on the Illumina HiSeq instruments: 2 × 76 bp and HiSeq 2500, 2 × 100 bp and HiSeq 2500 and 2 × 150 bp and HiSeq 4000, respectively.

QUANTIFICATION AND STATISTICAL ANALYSIS

Statistics—For statistical analysis between two groups, the two-tailed unpaired Student's t test and ANOVA test was used for parametric data. For non-parametric data, the Mann-Whitney U test was used instead. When more than two groups were compared, one-way ANOVA using Dunnett's analysis was used. P values < 0.05 were considered to indicate statistical significance.

Analysis of whole exome sequencing—Raw sequencing reads as in FASTQ files were processed and aligned to the mouse genome MGSCv37(mm9) using the Picard Tools at Broad Institute (http://broadinstitute.github.io/picard/), and the algorithm for read alignment was BWA (Li and Durbin, 2010). The BAM files were imported into the Broad FireCloud computing system (https://software.broadinstitute.org/firecloud/), and somatic SNVs and indels were called using the MuTect2 algorithm which is embedded in GATK (Van der Auwera et al., 2013). Mutations with less than 5 reads in tumor sample were excluded due to low-confidence mutation calls. Oncotator (Ramos et al., 2015) was used to perform functional annotation of mutations based on reference genome mm9. Exonic mutations including mis-sense, non-sense, silent, splice-site, non-stop, translation-start-site, in-frame, and frameshift mutations were accounted for calculation of mutation loads. Mutational signatures were obtained by deconvolution of all SNVs into separate components based on 96 distinct types of mutational base context, using the SignatureAnalyzer algorithm (Kim et al., 2016). A total of three mutational signatures were obtained and then compared to the COSMIC signatures (Tate et al., 2019), by cosine similarity. Two of the three mutational signatures were highly similar to COSMIC signature 11 and 26, respectively (similarity = 0.94 and 0.76), and COSMIC signature 11and 26 are associated with alkylating agents and defective DNA mismatch repair, respectively. Mutation loads associated with these two signatures account for 91.9% of all mutations.

Data and code availability—The DNA-seq data generated during this study are available at NCBI SRA database with number: PRJNA599415.

Supplementary Material

Refer to Web version on PubMed Central for supplementary material.

ACKNOWLEDGMENTS

We thank Dr. Theresa Swayne for taking 3D organoid images; Dr. Baojian Pan for pathological technical assistance; Mr. Karan Nagar for mouse colony maintenance; Ms. Kristie Gordon help FACS analysis in the CCTI Flow Cytometry Core (supported by NIH awards S10OD020056 and S10RR027050). Images analysis at the Microscopy Shared Resource of the Columbia University HICCC, supported by NIH/NCI grant P30 CA013696.

This research was supported by NIH grants (R35CA210088 and 5UO1DK103155) to TCW. WC was supported by National Natural Science Foundation (NSF) of China (81602035). HW was supported by the Shanghai Pujiang Program of China (16PJ1401900). HL and HD was supported by the NSF of China (81302079) and (81770624), respectively. JX was supported by Shanghai Engineering Research Center of Colorectal Cancer Minimally Invasive (17DZ2252600). YH is supported by JSPS, P-CREATE and PRIME from AMED, and Inoue Science Research Award.

REFERENCES

Ai W, Liu Y, Langlois M, and Wang TC (2004). Kruppel-like factor 4 (KLF4) represses histidine decarboxylase gene expression through an upstream Sp1 site and downstream gastrin responsive elements. J Biol Chem 279, 8684–8693. [PubMed: 14670968]

Alexandrov LB, Nik-Zainal S, Wedge DC, Aparicio SA, Behjati S, Biankin AV, Bignell GR, Bolli N, Borg A, Borresen-Dale AL, et al. (2013). Signatures of mutational processes in human cancer. Nature 500, 415–421. [PubMed: 23945592]

Arnold K, Sarkar A, Yram MA, Polo JM, Bronson R, Sengupta S, Seandel M, Geijsen N, and Hochedlinger K (2011). Sox2(+) adult stem and progenitor cells are important for tissue regeneration and survival of mice. Cell Stem Cell 9, 317–329. [PubMed: 21982232]

Asfaha S, Hayakawa Y, Muley A, Stokes S, Graham TA, Ericksen RE, Westphalen CB, von Burstin J, Mastracci TL, Worthley DL, et al. (2015). Krt19(+)/Lgr5(−) Cells Are Radioresistant Cancer-Initiating Stem Cells in the Colon and Intestine. Cell Stem Cell 16, 627–638. [PubMed: 26046762]

Barker N, Huch M, Kujala P, van de Wetering M, Snippert HJ, van Es JH, Sato T, Stange DE, Begthel H, van den Born M, et al. (2010). Lgr5(+ve) stem cells drive self-renewal in the stomach and build long-lived gastric units in vitro. Cell Stem Cell 6, 25–36. [PubMed: 20085740]

Bray F, Ferlay J, Soerjomataram I, Siegel RL, Torre LA, and Jemal A (2018). Global cancer statistics 2018: GLOBOCAN estimates of incidence and mortality worldwide for 36 cancers in 185 countries. CA Cancer J Clin 68, 394–424. [PubMed: 30207593]

Bu P, Chen KY, Chen JH, Wang L, Walters J, Shin YJ, Goerger JP, Sun J, Witherspoon M, Rakhilin N, et al. (2013). A microRNA miR-34a-regulated bimodal switch targets Notch in colon cancer stem cells. Cell Stem Cell 12, 602–615. [PubMed: 23642368]

Bultje RS, Castaneda-Castellanos DR, Jan LY, Jan YN, Kriegstein AR, and Shi SH (2009). Mammalian Par3 regulates progenitor cell asymmetric division via notch signaling in the developing neocortex. Neuron 63, 189–202. [PubMed: 19640478]

Buonamici S, Trimarchi T, Ruocco MG, Reavie L, Cathelin S, Mar BG, Klinakis A, Lukyanov Y, Tseng JC, Sen F, et al. (2009). CCR7 signalling as an essential regulator of CNS infiltration in T-cell leukaemia. Nature 459, 1000–1004. [PubMed: 19536265]

Cairns J (1975). Mutation selection and the natural history of cancer. Nature 255, 197–200. [PubMed: 1143315]

Choi W, Kim J, Park J, Lee DH, Hwang D, Kim JH, Ashktorab H, Smoot D, Kim SY, Choi C, et al. (2018). YAP/TAZ Initiates Gastric Tumorigenesis via Upregulation of MYC. Cancer Res 78, 3306–3320. [PubMed: 29669762]

Cicalese A, Bonizzi G, Pasi CE, Faretta M, Ronzoni S, Giulini B, Brisken C, Minucci S, Di Fiore PP, and Pelicci PG (2009). The tumor suppressor p53 regulates polarity of self-renewing divisions in mammary stem cells. Cell 138, 1083–1095. [PubMed: 19766563]

Demitrack ES, Gifford GB, Keeley TM, Carulli AJ, VanDussen KL, Thomas D, Giordano TJ, Liu Z, Kopan R, and Samuelson LC (2015). Notch signaling regulates gastric antral LGR5 stem cell function. EMBO J 34, 2522–2536. [PubMed: 26271103]

Dimaline R, and Varro A (2014). Novel roles of gastrin. J Physiol 592, 2951–2958. [PubMed: 24665102]

Feng R, Aihara E, Kenny S, Yang L, Li J, Varro A, Montrose MH, Shroyer NF, Wang TC, Shivdasani RA, et al. (2014). Indian Hedgehog mediates gastrin-induced proliferation in stomach of adult mice. Gastroenterology 147, 655–666 e659. [PubMed: 24859162]

Guo Z, and Ohlstein B (2015). Stem cell regulation. Bidirectional Notch signaling regulates Drosophila intestinal stem cell multipotency. Science 350, pii: aab0988 doi: 0910.1126/science.aab0988. [PubMed: 26586765]

Hayakawa Y, Ariyama H, Stancikova J, Sakitani K, Asfaha S, Renz BW, Dubeykovskaya ZA, Shibata W, Wang H, Westphalen CB, et al. (2015a). Mist1 Expressing Gastric Stem Cells Maintain the Normal and Neoplastic Gastric Epithelium and Are Supported by a Perivascular Stem Cell Niche. Cancer Cell 28, 800–814. [PubMed: 26585400]

Hayakawa Y, Chang W, Jin G, and Wang TC (2016). Gastrin and upper GI cancers. Current opinion in pharmacology 31, 31–37. [PubMed: 27591354]

Hayakawa Y, Fox JG, and Wang TC (2017). The Origins of Gastric Cancer From Gastric Stem Cells: Lessons From Mouse Models. Cell Mol Gastroenterol Hepatol 3, 331–338. [PubMed: 28462375]

Hayakawa Y, Jin G, Wang H, Chen X, Westphalen CB, Asfaha S, Renz BW, Ariyama H, Dubeykovskaya ZA, Takemoto Y, et al. (2015b). CCK2R identifies and regulates gastric antral stem cell states and carcinogenesis. Gut 64, 544–553. [PubMed: 24951258]

Ito T, Kwon HY, Zimdahl B, Congdon KL, Blum J, Lento WE, Zhao C, Lagoo A, Gerrard G, Foroni L, et al. (2010). Regulation of myeloid leukaemia by the cell-fate determinant Musashi. Nature 466, 765–768. [PubMed: 20639863]

Jin G, Ramanathan V, Quante M, Baik GH, Yang X, Wang SS, Tu S, Gordon SA, Pritchard DM, Varro A, et al. (2009). Inactivating cholecystokinin-2 receptor inhibits progastrin-dependent colonic crypt fission, proliferation, and colorectal cancer in mice. J Clin Invest 119, 2691–2701. [PubMed: 19652364]

Jin G, Westphalen CB, Hayakawa Y, Worthley DL, Asfaha S, Yang X, Chen X, Si Y, Wang H, Tailor Y, et al. (2013). Progastrin stimulates colonic cell proliferation via CCK2R- and beta-arrestin-dependent suppression of BMP2. Gastroenterology 145, 820–830 e810. [PubMed: 23891976]

Kiel MJ, H.S., Ashkenazi R, Gentry SN, Teta M, Kushner JA, Jackson TL, Morrison SJ. (2007). Haematopoietic stem cells do not asymmetrically segregate chromosomes or retain BrdU.. Nature 449, 238–242. [PubMed: 17728714]

Kim J, Mouw KW, Polak P, Braunstein LZ, Kamburov A, Kwiatkowski DJ, Rosenberg JE, Van Allen EM, D'Andrea A, and Getz G (2016). Somatic ERCC2 mutations are associated with a distinct genomic signature in urothelial tumors. Nat Genet 48, 600–606. [PubMed: 27111033]

Koh TJ, Goldenring JR, Ito S, Mashimo H, Kopin AS, Varro A, Dockray GJ, and Wang TC (1997). Gastrin deficiency results in altered gastric differentiation and decreased colonic proliferation in mice. Gastroenterology 113, 1015–1025. [PubMed: 9287997]

Lee Y, Urbanska AM, Hayakawa Y, Wang H, Au AS, Luna AM, Chang W, Jin G, Bhagat G, Abrams JA, et al. (2017). Gastrin stimulates a cholecystokinin-2-receptor-expressing cardia progenitor cell and promotes progression of Barrett's-like esophagus. Oncotarget 8, 203–214. [PubMed: 27448962]

Leushacke M, Ng A, Galle J, Loeffler M, and Barker N (2013). Lgr5(+) gastric stem cells divide symmetrically to effect epithelial homeostasis in the pylorus. Cell Rep 5, 349–356. [PubMed: 24209744]

Lew DJ, Burke DJ, and Dutta A (2008). The immortal strand hypothesis: how could it work? Cell Stem Cell 133, 21–23.

Li H, and Durbin R (2010). Fast and accurate long-read alignment with Burrows-Wheeler transform. Bioinformatics 26, 589–595. [PubMed: 20080505]

Li XB, Yang G, Zhu L, Tang YL, Zhang C, Ju Z, Yang X, and Teng Y (2016). Gastric Lgr5(+) stem cells are the cellular origin of invasive intestinal-type gastric cancer in mice. Cell Res 26, 838–849. [PubMed: 27091432]

Matsuo J, Kimura S, Yamamura A, Koh CP, Hossain MZ, Heng DL, Kohu K, Voon DC, Hiai H, Unno M, et al. (2017). Identification of Stem Cells in the Epithelium of the Stomach Corpus and Antrum of Mice. Gastroenterology 152, 218–231 e214. [PubMed: 27670082]

Morrison SJ, and Kimble J (2006). Asymmetric and symmetric stem-cell divisions in development and cancer. Nature 441, 1068–1074. [PubMed: 16810241]

Nakajima T, Konda Y, Izumi Y, Kanai M, Hayashi N, Chiba T, and Takeuchi T (2002). Gastrin stimulates the growth of gastric pit cell precursors by inducing its own receptors. Am J Physiol Gastrointest Liver Physiol 282, G359–366. [PubMed: 11804858]

Neumuller RA, and Knoblich JA (2009). Dividing cellular asymmetry: asymmetric cell division and its implications for stem cells and cancer. Genes & development 23, 2675–2699. [PubMed: 19952104]

Ohlstein B, and Spradling A (2007). Multipotent Drosophila intestinal stem cells specify daughter cell fates by differential notch signaling. Science 315, 988–992. [PubMed: 17303754]

Pellegrinet L, Rodilla V, Liu Z, Chen S, Koch U, Espinosa L, Kaestner KH, Kopan R, Lewis J, and Radtke F (2011). Dll1- and dll4-mediated notch signaling are required for homeostasis of intestinal stem cells. Gastroenterology 140, 1230–1240 e1231-1237. [PubMed: 21238454]

Potten CS, Owen G, and Booth D (2002). Intestinal stem cells protect their genome by selective segregation of template DNA strands. J Cell Sci 115, 2381–2388. [PubMed: 12006622]

Ramos AH, Lichtenstein L, Gupta M, Lawrence MS, Pugh TJ, Saksena G, Meyerson M, and Getz G (2015). Oncotator: cancer variant annotation tool. Hum Mutat 36, E2423–2429. [PubMed: 25703262]

Renz BW, Takahashi R, Tanaka T, Macchini M, Hayakawa Y, Dantes Z, Maurer HC, Chen X, Jiang Z, Westphalen CB, et al. (2018). beta2 Adrenergic-Neurotrophin Feedforward Loop Promotes Pancreatic Cancer. Cancer Cell 33, 75–90 e77. [PubMed: 29249692]

Reya T, Morrison SJ, Clarke MF, and Weissman IL (2001). Stem cells, cancer, and cancer stem cells. Nature 414, 105–111. [PubMed: 11689955]

Sakitani K, Hayakawa Y, Deng H, Ariyama H, Kinoshita H, Konishi M, Ono S, Suzuki N, Ihara S, Niu Z, et al. (2017). CXCR4-expressing Mist1(+) progenitors in the gastric antrum contribute to gastric cancer development. Oncotarget 8, 111012–111025. [PubMed: 29340033]

Sato T, van Es JH, Snippert HJ, Stange DE, Vries RG, van den Born M, Barker N, Shroyer NF, van de Wetering M, and Clevers H (2011). Paneth cells constitute the niche for Lgr5 stem cells in intestinal crypts. Nature 469, 415–418. [PubMed: 21113151]

Schorl C, and Sedivy JM (2007). Analysis of cell cycle phases and progression in cultured mammalian cells. Methods 41, 143–150. [PubMed: 17189856]

Shoshkes-Carmel M, Wang YJ, Wangensteen KJ, Toth B, Kondo A, Massasa EE, Itzkovitz S, and Kaestner KH (2018). Subepithelial telocytes are an important source of Wnts that supports intestinal crypts. Nature 557, 242–246. [PubMed: 29720649]

Sigal M, Logan CY, Kapalczynska M, Mollenkopf HJ, Berger H, Wiedenmann B, Nusse R, Amieva MR, and Meyer TF (2017). Stromal R-spondin orchestrates gastric epithelial stem cells and gland homeostasis. Nature 548, 451–455. [PubMed: 28813421]

Sigal M, Reines MDM, Mullerke S, Fischer C, Kapalczynska M, Berger H, Bakker ERM, Mollenkopf HJ, Rothenberg ME, Wiedenmann B, et al. (2019). R-spondin-3 induces secretory, antimicrobial Lgr5(+) cells in the stomach. Nat Cell Biol 21, 812–823. [PubMed: 31235935]

Sigal M, Rothenberg MD, Logan CY, Lee JY, Honaker RW, Cooper RL, Passarelli B, Camorlinga M, Bouley DM, Alvarez G, et al. (2015). Helicobacter pylori activates and expands Lgr5(+) stem cells through direct colonization of the gastric glands. Gastroenterology 147, 1392–1404.

Sugiarto S, Persson AI, Munoz EG, Waldhuber M, Lamagna C, Andor N, Hanecker P, Ayers-Ringler J, Phillips J, Siu J, et al. (2011). Asymmetry-defective oligodendrocyte progenitors are glioma precursors. Cancer Cell 20, 328–340. [PubMed: 21907924]

Takaishi S, Tu S, Dubeykovskaya ZA, Whary MT, Muthupalani S, Rickman BH, Rogers AB, Lertkowit N, Varro A, Fox JG, et al. (2009). Gastrin is an essential cofactor for helicobacter-

associated gastric corpus carcinogenesis in C57BL/6 mice. Am J Pathol 175, 365–375. [PubMed: 19556515]

Tate JG, Bamford S, Jubb HC, Sondka Z, Beare DM, Bindal N, Boutselakis H, Cole CG, Creatore C, Dawson E, et al. (2019). COSMIC: the Catalogue Of Somatic Mutations In Cancer. Nucleic Acids Res 47, D941–D947. [PubMed: 30371878]

Tian H, Biehs B, Warming S, Leong KG, Rangell L, Klein OD, and de Sauvage FJ (2011). A reserve stem cell population in small intestine renders Lgr5-positive cells dispensable. Nature 478, 255–259. [PubMed: 21927002]

Tomasetti C BI (2015a). The (not so) immortal strand hypothesis. Stem Cell Res 14, 238–241. [PubMed: 25700960]

Tomasetti C VB. (2015b). Cancer etiology. Variation in cancer risk among tissues can be explained by the number of stem cell divisions. Science 347, 78–81. [PubMed: 25554788]

Tomita H, Takaishi S, Menheniott TR, Yang X, Shibata W, Jin G, Betz KS, Kawakami K, Minamoto T, Tomasetto C, et al. (2011). Inhibition of gastric carcinogenesis by the hormone gastrin is mediated by suppression of TFF1 epigenetic silencing. Gastroenterology 140, 879–891. [PubMed: 21111741]

Van der Auwera GA, Carneiro MO, Hartl C, Poplin R, Del Angel G, Levy-Moonshine A, Jordan T, Shakir K, Roazen D, Thibault J, et al. (2013). From FastQ data to high confidence variant calls: the Genome Analysis Toolkit best practices pipeline. Curr Protoc Bioinformatics 43, 11 10 11–33. [PubMed: 25431634]

van Es JH, Sato T, van de Wetering M, Lyubimova A, Yee Nee AN, Gregorieff A, Sasaki N, Zeinstra L, van den Born M, Korving J, et al. (2012). Dll1+ secretory progenitor cells revert to stem cells upon crypt damage. Nature cell biology 14, 1099–1104. [PubMed: 23000963]

Wang TC, Dangler CA, Chen D, Goldenring JR, Koh T, Raychowdhury R, Coffey RJ, Ito S, Varro A, Dockray GJ, et al. (2000). Synergistic interaction between hypergastrinemia and Helicobacter infection in a mouse model of gastric cancer. Gastroenterology 118, 36–47. [PubMed: 10611152]

Westphalen CB, Asfaha S, Hayakawa Y, Takemoto Y, Lukin DJ, Nuber AH, Brandtner A, Setlik W, Remotti H, Muley A, et al. (2014). Long-lived intestinal tuft cells serve as colon cancer-initiating cells. J Clin Invest 124, 1283–1295. [PubMed: 24487592]

Zavros Y, Eaton KA, Kang W, Rathinavelu S, Katukuri V, Kao JY, Samuelson LC, and Merchant JL (2005). Chronic gastritis in the hypochlorhydric gastrin-deficient mouse progresses to adenocarcinoma. Oncogene 24, 2354–2366. [PubMed: 15735748]

Zavros Y, Rieder G, Ferguson A, Samuelson LC, and Merchant JL (2002). Genetic or chemical hypochlorhydria is associated with inflammation that modulates parietal and G-cell populations in mice. Gastroenterology 122, 119–133. [PubMed: 11781287]

Highlights

- Cck2r+ antral stem cells express Numb and divide asymmetrically
- Symmetric division by Cck2r+ cells is increased by MNU and suppressed by gastrin
- MNU treatment activates Notch signaling and thus decreases gastrin-secreting G cells
- Symmetric Cck2r+ cell division results in accumulation of gene mutations in tumors

Using lineage-tracing assays and paired cell analysis, Chang et al. show that murine $Cck2r^{+}$ +4 antral stem cells undergo predominant asymmetric division, and switch to symmetric division under carcinogenic stimulation. Tumorigenesis is associated with increased symmetric cell division that facilitates mutation and is suppressed by GPCR signaling.

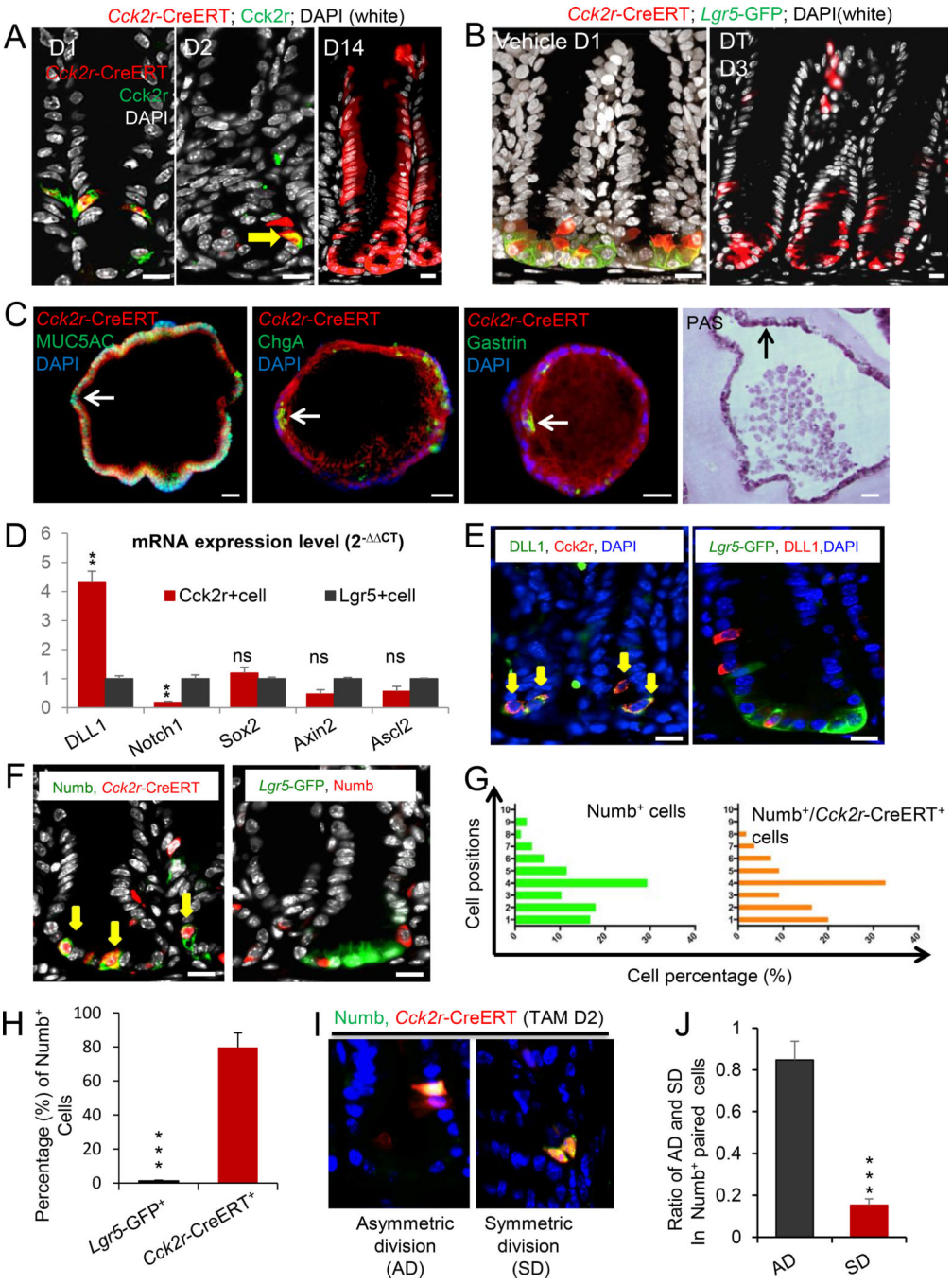

Figure 1. Antral +4 Cck2r$^+$ stem cells are DLL1$^+$ and Numb$^+$.

(A) *Cck2r* labels + 4 stem cells. Immunofluorescence of antral sections from induced *Cck2r*-CreERT;*R26*-tdTomato mice stained with DAPI (white), anti-Cck2r antibody (green), and tdTomato$^+$ (red). Day1 (left), Day 2 (middle), Day 14 (right). (B) Co-localization of Cck2r$^+$ cells (red) and Lgr5-GFP$^+$ cells (green) in the antrum of induced *Lgr5*-DTR-GFP;*Cck2r*-CreERT;*R26*-tdTomato mice on Day 1 without DT (left). Lineage tracing from Cck2r$^+$ antral cells at Day 3 after TAM and DT-mediated Lgr5$^+$ cell ablation (right). (C) Confocal images of immunostained organoids from single *Cck2r*$^+$ antral cells (red) from *Cck2r*-CreERT;R26-

tdTomato mice. Organoids were stained for MUC5AC (green), Chromogranin A (ChgA, green) or Gastrin (green). Left three panels: White arrows show positive immunostained cells. Right: arrow shows pit cells stained with periodic acid-Schiff (PAS red). (D) Cck2r$^+$ cells express DLL1. Relative mRNA expression (qPCR) levels of DLL1 and other genes in sorted single *Cck2r*-CreERT$^+$ cells and *Lgr5*-GFP$^+$ cells. Cells are sorted from *Cck2r*-CreERT;R26-tdTomato mice on Day 1 after TAM. Data are expressed as mean ± SD of three independent experiments. (E) Imunofluorescent staining of antral sections for DLL1 and Cck2r (left), and for DLL1 of *Lgr5*-DTR-GFP antral sections (right). Yellow arrows show double positive cells. (F) Cck2r$^+$ cells are Numb$^+$. Numb antibody staining of antral sections from *Cck2r*-CreERT;*R26*-tdTomato mice (left; n=4) and *Lgr5*-DTR-GFP mice (right; n=4). Mice were sacrificed 24h after TAM. Yellow arrows show double positive cells. (G) Quantitation by cell position of Numb$^+$ cells and Numb$^+$*Cck2r*-CreERT$^+$ cells in antral glands at 24h after TAM of *Cck2r*-CreERT;*R26*-tdTomato mice (n=4). Twenty-five antral glands were analyzed per mouse. Data are expressed as mean ± SD. (H) The percentage of Numb$^+$ cells in *Cck2r*-CreERT$^+$ cells (n=100) and *Lgr5*-GFP$^+$ cells (n=100), based on immunostaining from *Cck2r*-CreERT;*R26*-tdTomato and *Lgr5*-DTR-GFP mice. Data are expressed as mean ± SD. (I) Representative images of *Cck2r*-CreERT$^+$ traced paired-cells with Numb immunostaining from antral sections of *Cck2r*-CreERT;*R26*-tdTomato mice (n=4), showing segregation of Numb protein at Day 2 after TAM. (J) The proportion of asymmetric (AD, black) and symmetric (SD, red) cell division in *Cck2r*-CreERT$^+$/Numb$^+$ paired-cells in antral glands *in vivo* from *Cck2r*-CreERT;*R26*-tdTomato mice (n=3). Data are expressed as mean ± SD of 150 paired cells from three mice. Scale bars represent 25μm (C) and 10μm (A, B, E, F and I). *P<0.05, **P<0.01, ***P<0.001. See also Figure S1.

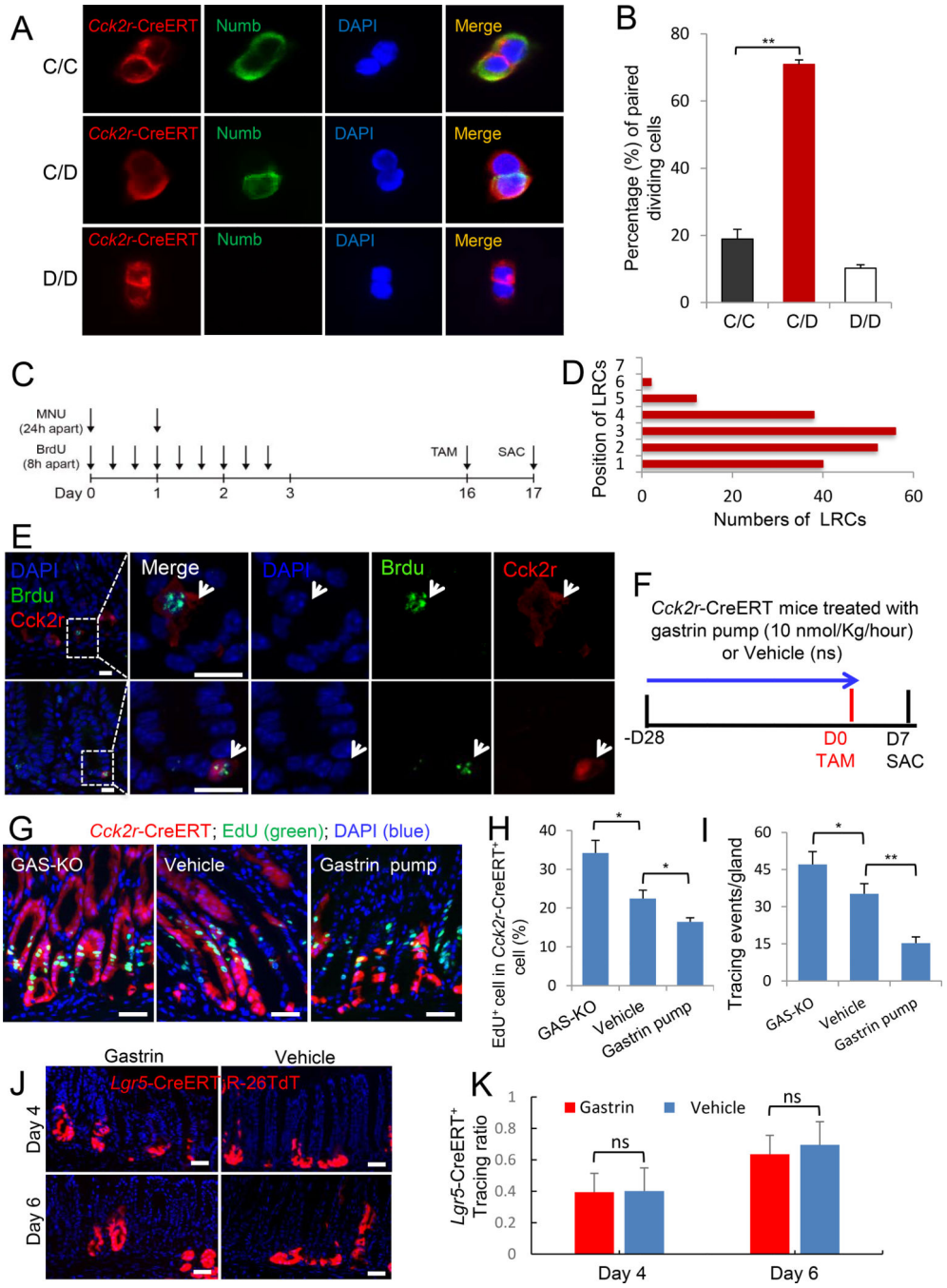

Figure 2. Antral +4 stem cells are label retaining cells, undergo asymmetric cell division, and are regulated by gastrin.

(A) *Cck2r*-CreERT^{+} cells undergo predominant asymmetric cell division. *Cck2r*-CreERT^{+} antral cells from *Cck2r*-CreERT;*R26*-tdTomato mice were sorted as single cells, cultured *in vitro,* and paired-cells then analyzed using immunofluorescent staining for Numb (green) (Bu et al., 2013; Bultje et al., 2009). (B) The percentage of Cck2r^{+} stem cells undergoing symmetric division (Numb^{+}/Numb^{+}, C/C; 18.9%), asymmetric division (Numb^{+}/Numb^{-}, C/D; 70.8%) and two Numb^{-} (D/D; 10.3%) in Figure 2A. Data are expressed as mean ± SD of three independent experiments, and a total 106 *Cck2r*-CreERT^{+} paired-cells were

analyzed. (C) Schematic diagram of the BrdU label retaining protocol in *Cck2r*-CreERT;*R26*-tdTomato mice (n=6). BrdU was given by i.p. injection every 8 hours over 3 days, along with 2 oral gavages of MNU. Following a 2 weeks' washout period and 24h after TAM, BrdU staining was performed on antral sections. (D) Quantitation by cell position of $BrdU^+$ label retaining cells (LRCs) in the gastric antrum. (E) Representative images of $Brdu^+/Cck2r^+$ LRCs in the gastric antrum of *Cck2r*-CreERT;*R26*-tdTomato mice. (F) Schematic diagram showing the protocol for gastrin infusion via osmotic pump, followed by TAM. (ns: nature saline) (G) Immunostaining for EdU (green) in *Cck2r*-CreERT;*R26*-tdTomato mice treated with vehicle (middle), gastrin pump (10 nmol/Kg/hour, for 4 weeks) (right), and crossed to GAS-KO mice (left). Lineage tracing (red) from $Cck2r^+$ cells was observed at day 7 after TAM (n=4 mice per group). (H-I) Quantification of EdU^+ labeled cells (shown in G) as a percentage (%) of *Cck2r*-$CreERT^+$ traced cells per antrum gland (H) and linage tracing events per gland from *Cck2r*-$CreERT^+$ cells (I) in the three groups of mice. Ten antral glands were analyzed per mouse. Data are expressed as mean ± SD. (J) Lineage tracing from *Lgr5*-CreERT;*R26*-tdTomato mice treated with gastrin infusion (10 nmol/Kg/hour) or vehicle at day 4 (n=4) and day 6 (n=4) after induction. (K) Quantification of tracing ratio of *Lgr5*-$CreERT^+$ cells in (I). Twenty-five antral glands are analyzed per mouse. Data are expressed as mean ± SD. Scale bars represent 10 μm (E) and 50 μm (G, J). *P<0.05, **P<0.01. See also Figure S2.

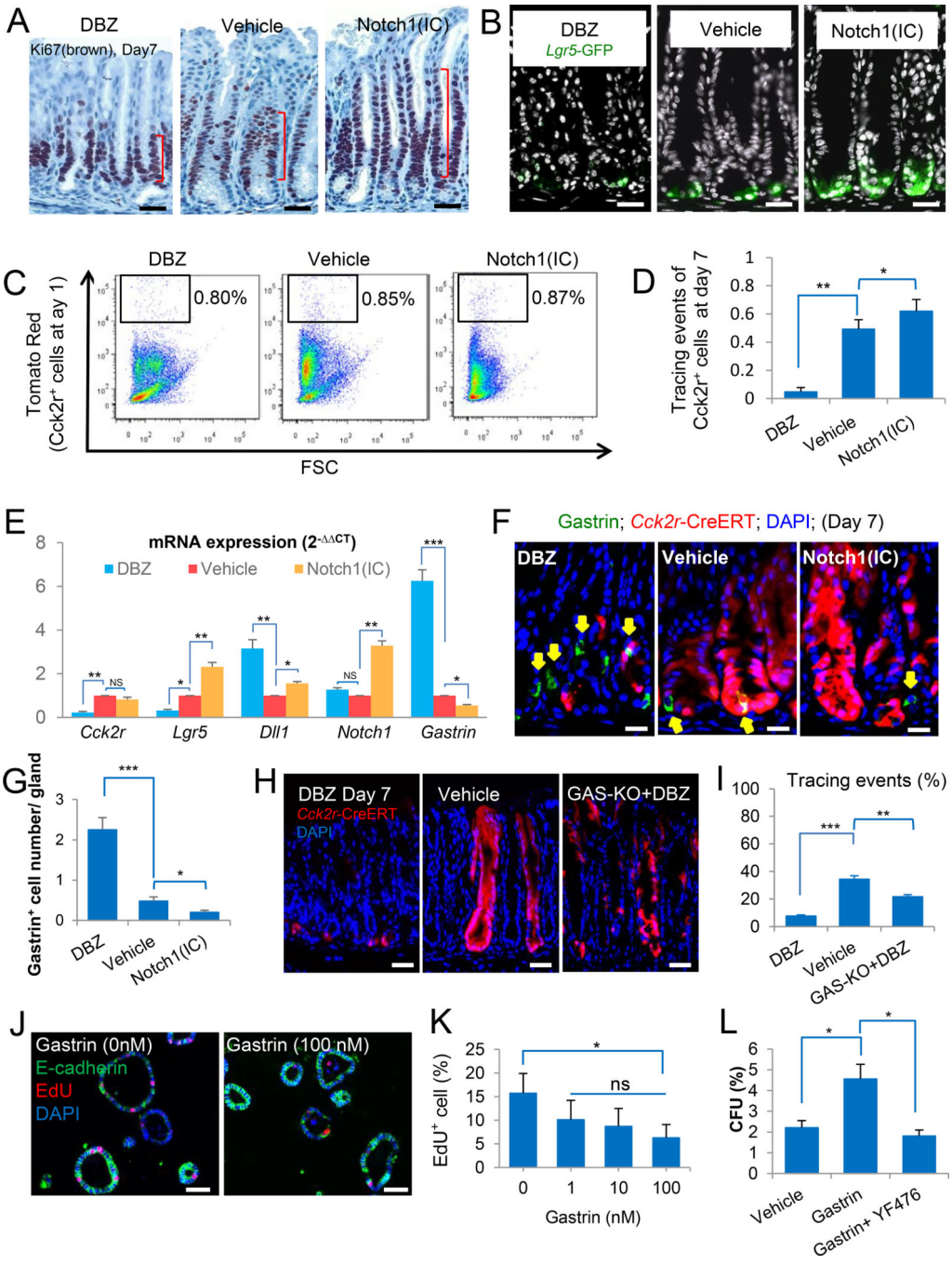

Figure 3. Antral +4 stem cells are regulated by Notch indirectly through niche gastrin cells.

(A) Representative images of Ki67 stained antral epithelium in vehicle treated mice, DBZ treated mice (5 doses) and *Eef1a1*-LSL-*Notch1(IC)* mice (Notch1(IC) mice). Each group had 4 mice. (B) Immunofluorescent images of DAPI-stained antral gastric sections from *Lgr5*-DTR-GFP mice treated with vehicle or DBZ, or *Lgr5*-DTR-GFP crossed to Notch1(IC) mice (n=4 per group). (C) Quantification by FACS of Cck2r$^+$ cells after Notch modulation in *Cck2r*-CreERT;*R26*-tdTomato mice. FACS plots showing relative numbers of Cck2r$^+$ cells (red) in vehicle treated mice, DBZ treated mice or *Cck2r*-CreERT crossed to

Notch1(IC) mice at 24h after TAM. (D) Quantification of lineage tracing events/gland in *Cck2r*-CreERT;*R26*-tdTomato mice treated with DBZ or vehicle, or crossed to Notch1(IC) mice on Day 7 after TAM (n=4 per group). (E) *Cck2r*, *Lgr5*, *Dll1*, *Notch1* and *Gastrin* gene expression levels as measured by qPCR in three groups of mice from (D). data are expressed as mean ± SD. (F) Representative images of antral sections from *Cck2r*-CreERT;*R26*-tdTomato mice immunostained for gastrin (green) and DAPI (blue). Mice were treated with DBZ or vehicle, or crossed to Notch1(IC) mice on Day 7 after TAM (n=4 per group). (G) Quantification of gastrin$^+$ cell numbers in the three groups of mice from (F). Twenty-five antral glands are analyzed per mouse. (H) Representative lineage tracing at day 7 post-TAM in *Cck2r*-CreERT;*R26*-tdTomato mice treated with DBZ, vehicle, or with DBZ after crosses to GAS-KO mice, n=4 per group. (I) Quantification of Cck2r tracing events per gland in the three groups of mice in (H). Twenty-five antral glands are analyzed per mouse. (J) Gastrin suppresses proliferation of antral spheroids in 3D culture in vitro. Representative images of double staining for E-cadherin (green) and EdU (red) of antral spheroids cultured with or without gastrin (G-17, 0 nM or 100 nM). (K) Quantification of the percentage of EdU$^+$ cells in response to four different gastrin concentrations. Data are expressed as mean ± SD of three independent experiments. (L) Effect of gastrin on colony-forming unit (CFU) efficiency from single *Cck2r*-CreERT$^+$ cells. CFU was calculated for each of the three groups as the percentage of colonies/ total number of seeded cells. The three groups included Cck2r$^+$ cells treated with vehicle, gastrin (100 nM), or gastrin + YF476 (1 uM) in the culture medium, respectively. Data are expressed as mean ± SD of three independent experiments. Scale bars represent 50 μm (J), 25 μm (A, B, H and K) and 10 μm (F). *P<0.05, **P<0.01, ***P<0.001. See also Figure S2, S3.

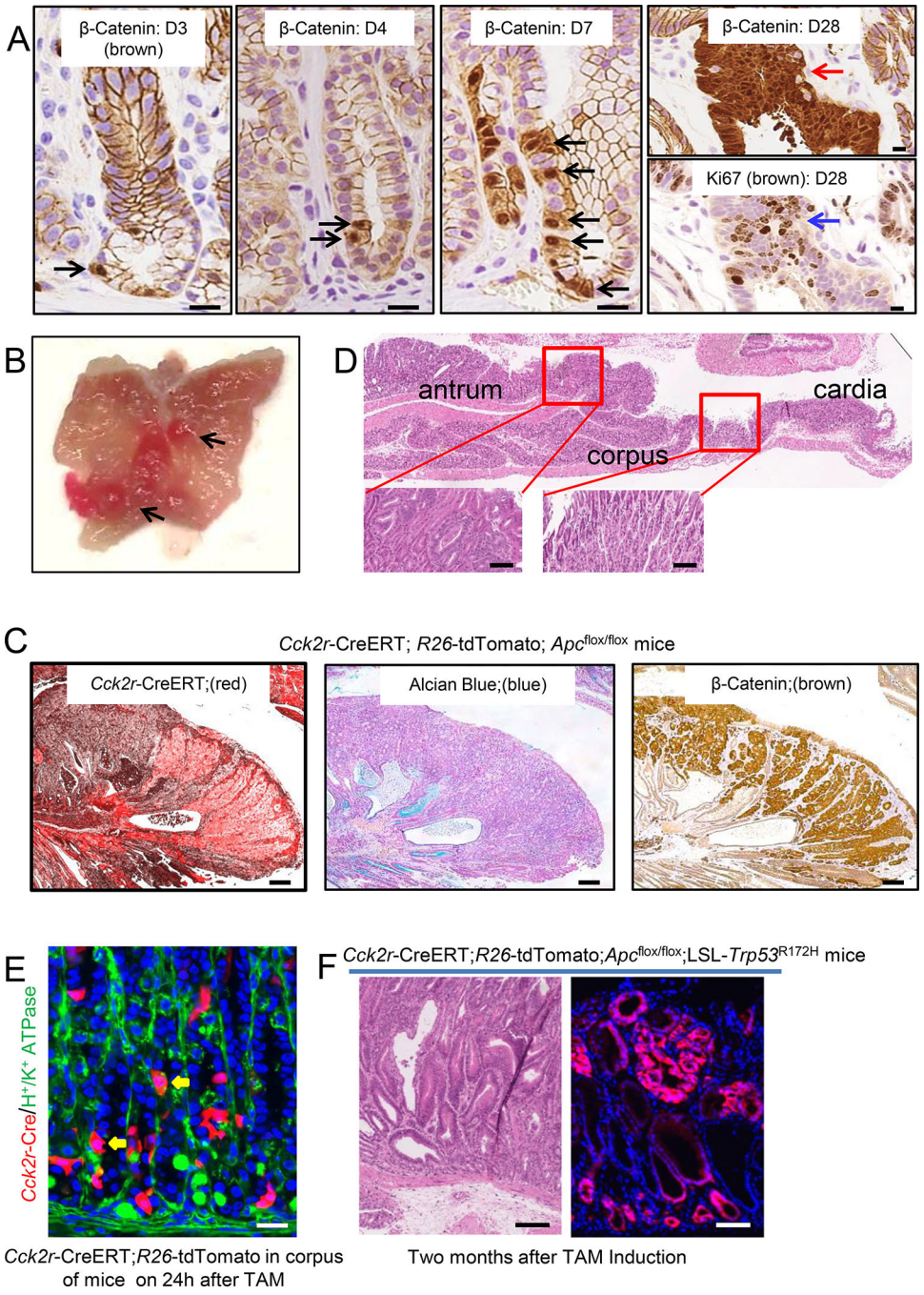

Figure 4. Cck2r^{+} cells give rise to intestinal-type metaplasia and cancer

(A) Beta-catenin immunohistochemical staining of antral sections from *Cck2r*-CreERT;*Rd* 26-tdTomato;*Apc*$^{flox/flox}$ mice at Day 3 to Day 28 after TAM. Black arrows show accumulation of β-catenin (brown). Red arrows indicate β-catenin^{+} gastric adenomas, which express high levels of Ki67 (blue arrow). (B) Gross image of macroscopic tumors (black arrow) from *Cck2r*-CreERT;*R26*-tdTomato;*Apc*$^{flox/flox}$ mice at 4 month after TAM. (C) Representative images of antral sections from *Cck2r*-CreERT;*R26*-tdTomato;*Apc*$^{flox/flox}$ mice at 4 months post TAM. TdTomato lineage tracing (left, red), Alcian Blue staining

(middle, blue), and β-catenin immunostaining (right, brown) in tumors. (D) H&E staining of antral sections from *Cck2r*-CreERT;*R26*-tdTomato;*Apc*$^{flox/flox}$ mice at 4 months after TAM. Inset boxes show high power magnification, demonstrating dysplasia in antrum glands. (E) Representative immunofluorescence image from corpus gland in *Cck2r*-CreERT;*R26*-tdTomato mice at 24h after TAM, showing abundant single recombined cells (in red), with immunostaining for H/K-ATPase-expressing parietal cells shown in green. Yellow arrows indicate Cck2r-expressing parietal cells. (F) Representative H&E stained section (left) and immunofluorescence image (right) from *Cck2r*-CreERT;*R26*-tdTomato;*Apc*$^{flox/flox}$; LSL-*Trp53*^{R172H} mice at 2 month after TAM. Scale bars represent 10 μm (A, D, F), and 50 μm (B, E), and 100 um (C). Data are expressed as mean ± SD; * $P<0.05$, ** $P<0.01$, *** $P<0.001$.

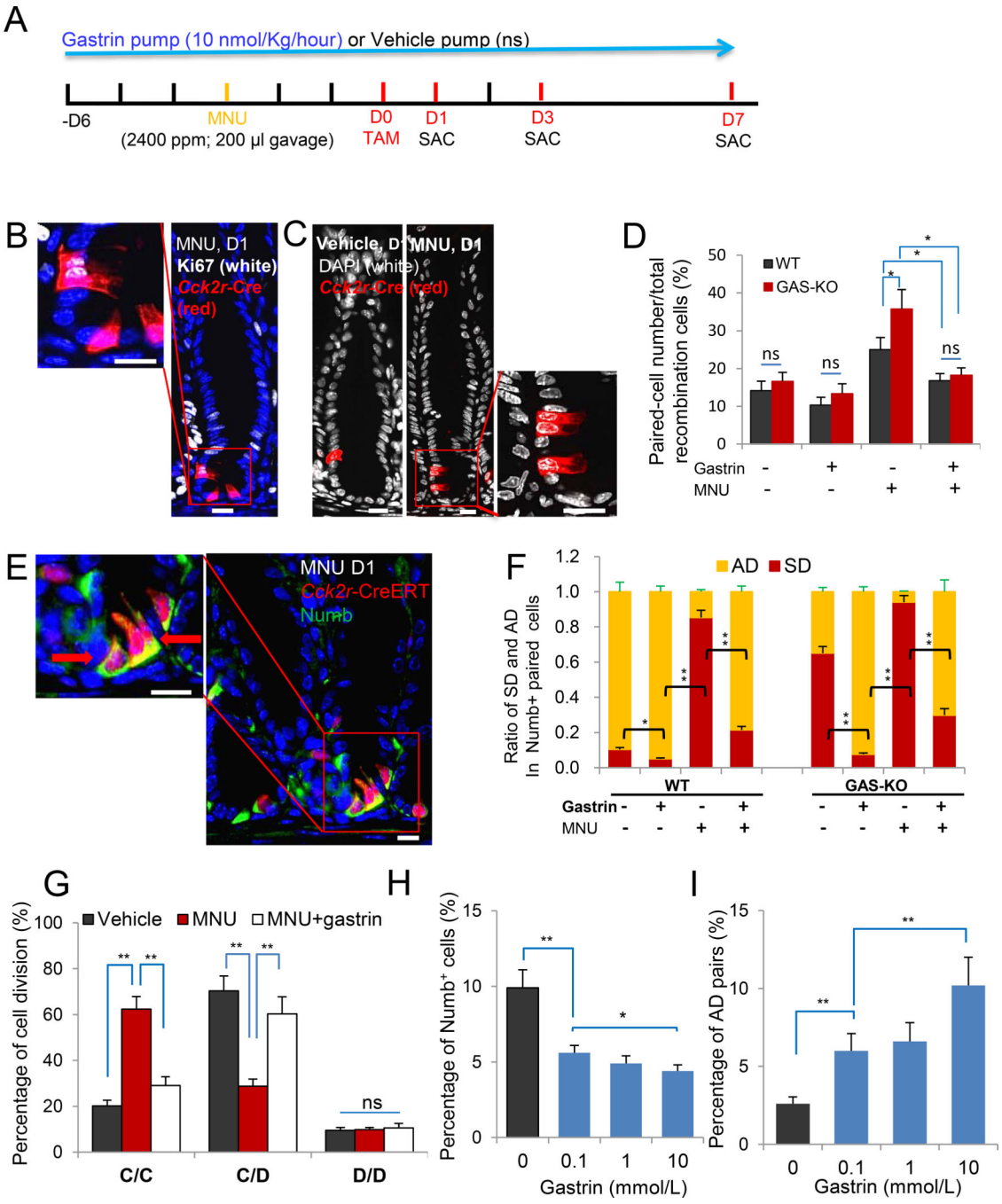

Figure 5. Gastric carcinogenesis promotes Cck2r^{+} symmetric cell division and stem cell expansion, which are suppressed by gastrin.

(A) Schematic diagram of protocol used for carcinogenesis studies in *Cck2r*-CreERT mice. Mice were treated with vehicle, MNU or gastrin, or both MNU and gastrin, and sacrificed at D1, D3 and D7 after TAM. (B) Representative immunofluorescent images of antral glands showing *Cck2r*-CreERT^{+} paired cells (red) with Ki67 antibody staining (white) at 24 hours after TAM and MNU treatment. DAPI (blue). (C) Representative immunofluorescence images of antral glands from *Cck2r*-CreERT;*R26*-tdTomato mice showing paired cells (red) at 24 hours after TAM, with MNU or without MNU (Vehicle) treatment. DAPI (white). Inset

shows higher power image of paired cells. (D) The ratio (or percentage) of *Cck2r*-CreERT^{+} paired cells over the total recombined cells in *Cck2r*-CreERT;*R26*-tdTomato mice and GAS-KO; *Cck2r*-CreERT;*R26*-tdTomato mice, when treated with gastrin, MNU, neither or both. and twenty-five antral glands were analyzed for each mouse, n=4 per group. Data are expressed as mean ± SD. (E) Representative immunofluorescent images of antral glands from *Cck2r*-CreERT;*R26*-tdTomato mice showing *Cck2r*-CreERT^{+} paired cells with Numb staining (green), with symmetric cell division (red arrows) at 24 hours after TAM and MNU treatment. Inset shows higher power image of paired cells. (F) Proportion of symmetric division (SD, red) and asymmetric division (AD, yellow) among *Cck2r*-CreERT^{+}/Numb^{+} paired cells in Numb-stained antral gland sections from *Cck2r*-CreERT;*R26*-tdTomato (WT) mice and GAS-KO; *Cck2r*-CreERT;*R26*-tdTomato mice. Mice were treated with gastrin infusion, MNU, neither or both, and sacrificed at 24 hours after TAM. Total 100 paired-cells were analyzed for each mouse, n=4 per group. Data are expressed as mean ± SD. (G) Effect of MNU on cell division of single sorted Cck2r^{+} cells *in vitro* by paired-cell analysis. Bar graph showing the relative proportion of cell pairs with two Numb^{+} (C/C), one Numb^{+} (C/D) or two Numb^{-} (D/D) cells, following in vitro culture and Numb immunostaining. *Cck2r*-CreERT;*R26*-tdTomato mice were divided into three groups (vehicle, MNU treatment and MNU + gastrin treatment, n=4 per group). *Cck2r*-tdTomato^{+} cells were isolated by FACS, and paired-cells were analyzed from vehicle-treated mice (n=75 paired cells), MNU-treated mice (n=45 paired cells), MNU plus gastrin mice (n=40 paired cells). (H) The effect of gastrin on number of Numb^{+} AGS-E cells following in vitro culture. Data are expressed as mean ± SD of three independent experiments. (I) Effect of gastrin on the percentage of asymmetric divisions (AD) in AGS-E paired-cells based on Numb immunostaining. Data are expressed as mean ± SD of three independent experiments and total 45, 50, 40 and 45 AGS-E paired-cells were calculated for gastrin 0, 0.1, 1 and 10 mmol/L, respectively. Scale bars represent 100 μm (A) and 10 μm (B, C and E). *P<0.05, **P<0.01, ***P<0.001. See also Figure S5.

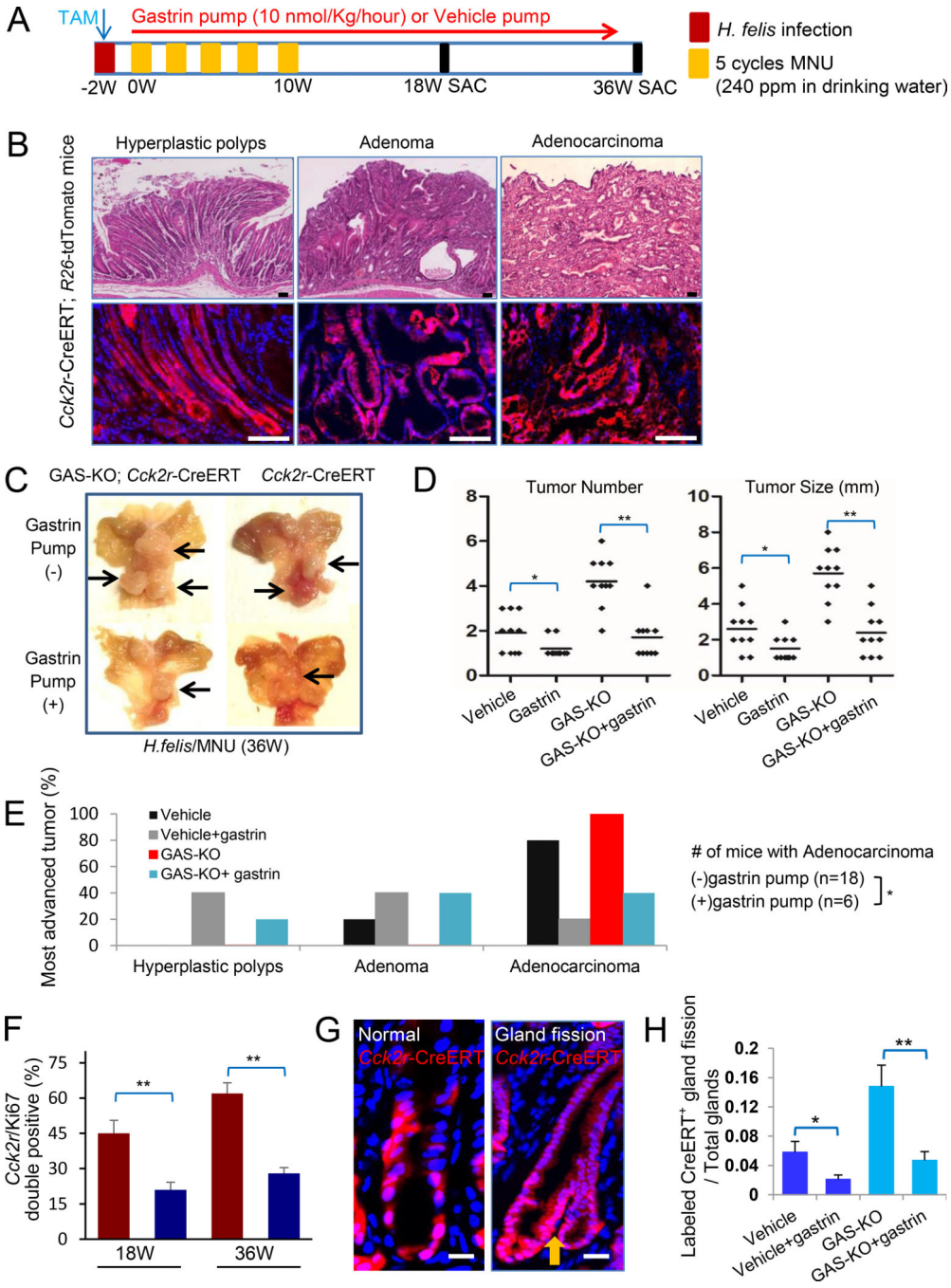

Figure 6. Antral gastric mutagenesis and tumorigenesis are suppressed by gastrin.

(A) Schematic diagram of experimental protocol that includes TAM induction, *H. felis* infection, MNU treatment, and gastrin infusion in *Cck2r*-CreERT;*R26*-tdTomato mice and GAS-KO;*Cck2r*-CreERT; *R26*-tdTomato mice. (B) Histopathologic features with lineage tracing of gastric tumors in MNU-treated *Cck2r*-CreERT;*R26*-tdTomato mice at 36 weeks. Top shows H&E stained sections, while bottom show immunofluorescence microscopy images of tdTomato expression. Hyperplastic polyp (left); Adenoma (middle); Adenocarcinoma (right). (C) Representative gross images of resected stomachs with tumors

from *Cck2r*-CreERT mice and GAS-KO;*Cck2r*-CreERT mice treated with *H. felis* infection and 5 cycles of MNU. Mice from each genotype were treated with either a gastrin pump or a vehicle pump, and sacrificed at 36 weeks after start of MNU, n=10 per group. (D) Tumor number (left) and maximum tumor size (right) from the four groups of mice shown in (C). (E) Proportion of mice with the most advanced histopathology in the four groups of mice shown in (C). Mice were classified according to the histologic grade of the most advanced tumor. (F) The percentage of $Cck2r^+$ cells that were also $Ki67^+$ (i.e. double positive cells) from GAS-KO;*Cck2r*-CreERT; *R26*-tdTomato mice, induced with tamoxifen and treated with *H. felis* infection and 5 cycles of MNU gavage. Mice received infusion with either gastrin pump (blue) or vehicle pump (red), and were sacrificed at 18 or 36 weeks. Ten random high power filed are analyzed per mouse, n=3 per group. Data are expressed as mean ± SD. (G) Representative immunofluorescence images of *Cck2r*-CreERT;*R26*-tdTomato glands following TAM. Left shows normal antral gland with lineage tracing, while right shows representative $Cck2r^+$ cell-derived crypt fission image (yellow arrow). (H) The ratio of CreERT-traced gland fission events per total glands in the four groups of mice. *Cck2r*-CreERT mice and GAS-KO;*Cck2r*-CreERT mice were treated with gastrin pump or vehicle and analyzed 18 weeks after the start of MNU treatment. Total 50 labelled crypts per mouse were measured. Data are expressed as mean ± SD. Scale bars represent 50 μm (B) and 10 μm (G). *P<0.05, **P<0.01. See also Figure S6.

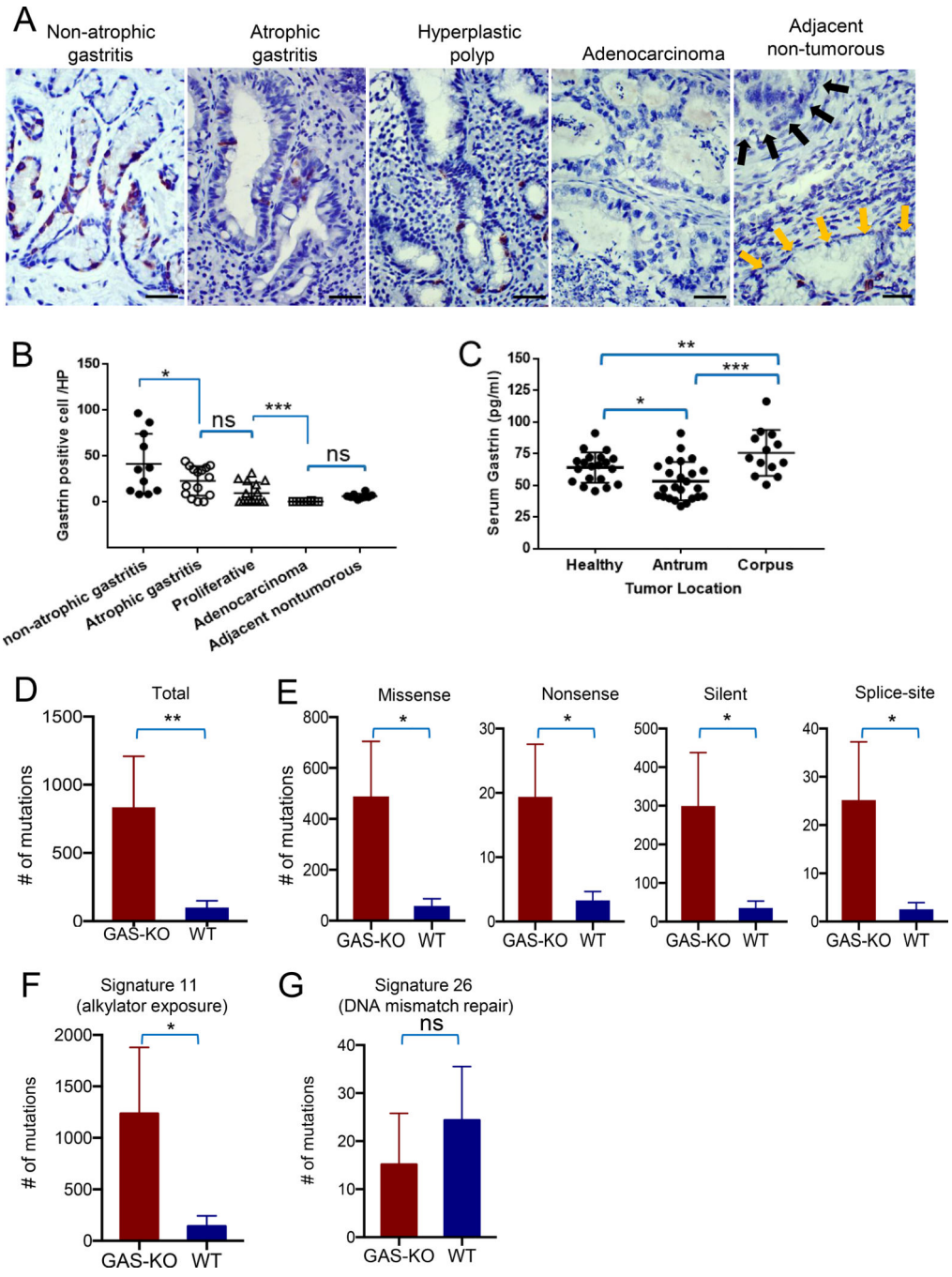

Figure 7. Decreased gastrin expression is associated with progression of human gastric antral neoplasia.

(A) Immunohistochemical expression of gastrin in gastric antral preneoplastic lesions and gastric antral cancer. Patients with non-atrophic gastritis (n=10), atrophic gastritis (n=15), hyperplastic polyp (n=15), adenocarcinoma (n=10). Right panel shows a section of adjacent nontumorous tissue with rare gastrin^{+} cells (yellow arrows), while tumor is shown with black arrows. (B) Quantification of gastrin^{+} cells per high power field in the four groups of patients shown in (A). (C) Relationship between serum gastrin level and tumor location in patients with gastric cancer. Dot plot graph show gastrin levels (pg/ml) in patients with

corpus cancer (n=13), antrum cancer (n=24), and healthy controls (n=20). (D) The average number of mutations in tumors from GAS-KO (n=5) and WT mice (n=7), based on exome sequencing. (E) Spectrum of mutations in antral tumors developing in GAS-KO mice compared to WT mice. Bar graph showing quantification and comparisons of major classes (missense, silence, nonsense and splice site) of exome mutations in antral tumors between GAS-KO (n=5) and WT (n=7) mice. (F, G) Bar graph showing quantification of mutations for two prominent COSMIC mutational signatures in GAS-KO (n=5) versus WT (n=7) antral tumors. Scale bars represent 50 μm (A). Data are expressed as the mean ± SD * P<0.05, ** P<0.01, *** P<0.001. See also Figure S6.

KEY RESOURCES TABLE

REAGENT or RESOURCE	SOURCE	IDENTIFIER
Antibodies		
Anti-Ki67 Antibody	Abcam	Cat#: ab16667 RRID: AB_302459
Anti-GFP Antibody	Abcam	Cat#: ab13970 RRID: AB_300798
RFP Antibody Pre-adsorbed	Rockland Immunochemicals	Cat#: 600-401-379 RRID: AB_2209751
H^+/K^+ ATPase Antibody (C-4)	Santa Cruz Biotechnology Biotechnology	Cat#: sc-374094, RRID:AB_10917224
Mucin 5AC Antibody (K-20)	Santa Cruz Biotechnology	Cat# sc-16903, RRID:AB_649616
Somatostatin Antibody	Abcam	Cat# ab30788, RRID:AB_778010
Gastrin Antibody (C-20)	Santa Cruz Biotechnology	Cat# sc-7783, RRID:AB_2108261
Anti-DLL1 Antibody	Abcam	Cat# ab10554, RRID:AB_2092808
Anti-NUMB Antibody	Abcam	Cat# ab14140, RRID:AB_443023
Trefoil Factor 2 (TFF2) Antibody	Antibodies-online	Cat# ABIN351426, RRID:AB_10826089
Human Gastrin Antibody	Abcam	Cat#: ab22622, RRID:AB_447203
CCK-BR Antibody (C-18)	Santa Cruz Biotechnology	Cat# sc-16177, RRID:AB_2070493
Rat anti-E-Cadherin (Mouse)	Innovative Research	Cat# 13-1900, RRID:AB_86571
Intrinsic Factor Antibody	Santa Cruz Biotechnology	Cat# sc-161643, RRID:AB_10839153
DCKL1 Antibody (C-term)	Abgent	Cat# AP7219b, RRID:AB_2090081
BrdU Antibody	Abcam	Cat# ab6326, RRID:AB_305426
Rabbit Anti-activated Notch1 Polyclonal Antibody	Abcam	Cat# ab8925, RRID:AB_306863
E-cadherin Antibody	Cell Signaling Technology	Cat# 3195, RRID:AB_2291471
β-Catenin Antibody	BD Bioscience	Cat# 610153, RRID:AB_397554
EnVision+ System-HRP (DAB)	DAKO	Cat#: K4011
Anti-Chromogranin A Antibody (ab15160)	Abcam	Cat# ab15160, RRID:AB_301704
Anti-Hes1 Antibody (ab71559)	Abcam	Cat# ab71559, RRID:AB_1209570
Alexa Fluor 647 Donkey Anti-Rabbit	Abcam	Cat# ab150075, RRID:AB_2752244
Alexa Flour 488 Chichen Anti-Goat	Life technologies	Cat#: A-21467
Alexa Fluor 488 Goat Anti-Chicken	Thermo Fisher Scientific	Cat# A-11039, RRID:AB_2534096
Alexa Fluor 594 Goat Anti-Rabbit	Thermo Fisher Scientific	Cat# R37117, RRID:AB_2556545
Alexa Fluor 488 Chicken Anti-Rabbit	Thermo Fisher Scientific	Cat# A-21441, RRID:AB_2535859
Alexa Fluor 594 Chicken Anti-Goat	Thermo Fisher Scientific	Cat# A-21468, RRID:AB_2535871
Alexa Fluor 647 Phalloidin	Thermo Fisher Scientific	Cat# A22287, RRID:AB_2620155
Alexa Fluor 555 Goat Anti-Chicken	Thermo Fisher Scientific	Cat# A-21437, RRID:AB_2535858
Alexa Fluor 555 Goat Anti-Mouse	Thermo Fisher Scientific	Cat# A-21422, RRID:AB_2535844
Bacterial and Virus Strains		
Bacterial: Helicobacter felis	N/A	Strains: ATCC 49179
Biological Samples		
Human Blood Samples	Zhongshan Hospital	N/A

REAGENT or RESOURCE	SOURCE	IDENTIFIER
Human Gastric Samples	Zhongshan Hospital	N/A
Chemicals, Peptides, and Recombinant Proteins		
HBSS – Hank's Balanced Salt Solution	Gibco	14175079
DPBS, no calcium, no magnesium	Gibco	14190250
Advanced DMEM/F12	Gibco	12634010
Fetal Bovine Serum	Gibco	16140071
Collagenase, Type 4	Worthington Biochemical Corporation	LS004186
DNase I	Thermo Fisher Scientific	3724778103
BD Horizon BrilliantTM Stain Buffer	BD Biosciences	563794
DAPI Solution	BD Pharmingen	564907
B-27® Supplement (50X), serum free	Thermo Fisher Scientific	17504-044
N-2 Supplement (100X)	Thermo Fisher Scientific	17502-048
Matrigel® Growth Factor Reduced (GFR) Basement Membrane Matrix	Corning	356231
Gastrin	Sigma-Aldrich	G9145
IntestiCult™ Organoid Growth Medium (Mouse)	STEMCELL Technologies	6005
RNAlater® Stabilization Solution	Thermo Fisher Scientific	AM7020
Mouse Gastrin EIA	RayBiotech	EIAM-GAS-1
Insulin growth factors	STEMCELL Technologies	2742
BIRB-796 (p38 MAPK inhibitor)	STEMCELL Technologies	72682
IntestiCult™ Organoid Growth Medium (Mouse)	STEMCELL Technologies	6005
Gamma-secretase inhibitor (DBZ)	RD Systems	4489/10
Diphtheria Toxin	Sigma-Aldrich	D0564-1MG
BrdU (5-Bromo-2'-deoxyuridine)	Sigma-Aldrich	B5002-5G
EdU (5-ethynyl-2'-deoxyuridine)	Life Technologies	A10044
HEPES	Thermo Fisher Scientific	15630-080
TrypLE™ Express Enzyme (1X), phenol red	Thermo Fisher Scientific	12605-028
MNU (N-methyl-N-nitrosourea)	Gojira Fine Chemicals	NM1003
Tamoxifen	Sigma-Aldrich	T5648-5G
GlutaMAX™ Supplement	Thermo Fisher Scientific	35050-079
Gentamicin	Thermo Fisher Scientific	SR0185E
Penicillin-Streptomycin (10,000 U/mL)	Thermo Fisher Scientific	15140-122
N-acetylcysteine	Sigma-Aldrich	A9165-5G
EDTA	Sigma-Aldrich	431788-25G
A83-01	Sigma-Aldrich	909910-43-6
Poly-L-lysine	Sigma-Aldrich	25988-63-0
Y-27632	Sigma-Aldrich	Y0503-1MG
Nicotinamide	Sigma-Aldrich	N0636-100G
Recombinant Murine Noggin	Peprotech	250-38
Recombinant Human FGF-10	Peprotech	100-26

REAGENT or RESOURCE	SOURCE	IDENTIFIER
Recombinant Human R-Spondin-1	Peprotech	120-38
Recombinant Murine WNT-3a	Peprotech	315-20B
Recombinant Murine EGF	Peprotech	315-09
UltraPure™ DNase/RNase-Free Distilled Water	Thermo Fisher Scientific	10977-023
Hydrogen peroxide solution 30 % (w/w) in H2O, contains stabilizer	Sigma-Aldrich	H1009-500ML
Collagenase type I (0.25%)	STEMCELL Technologies	07902
Acta lube	Pharmacy	NDC 198-50
Diphtheria Toxin	Sigma-Aldrich	D0564-1MG
Falcon Yellow Nylon Mesh Cell Strainer, 70 Micron	BD Biosciences	352350
Falcon Blue Nylon Mesh Cell Strainer, 40 Micron	BD Biosciences	352340
Alzet pump Model 2006 (0.15 μl/hr, 6 weeks)	Alzet	7223
Alzet pump Model 1002 (0.25 μl/hr, 2 weeks)	Alzet	4317
Alzet pump Model 1007D (0.5 μl/hr, 7 days)	Alzet	290
48-well Uncoated glass dish	MatTek	P48G-1.5-6-F Case
35 mm Collagen Coated dish	MatTek	P35GCOL-0-10-C Case
ImmEdge Hydrophobic Barrier Pen	Vector	H-4000
Critical Commercial Assays		
NucleoSpin tissue kit (Macherey-Nagel)	Macherey-Nagel	740952
Nucleospin RNA II kit	Clontech Laboratories	740468.4
Human Gastrin ELISA Kit	Abcam	ab133033
Click-iT® EdU Imaging Kit with Alexa Fluor® 488, 594, and 647 Azides	Life Technologies	C10086
Click-iT® EdU Alexa Fluor® 488 Imaging Kit	life technologies	C10337
MTT assay Kit	Thermo Fisher Scientific	V13154
Nextera XT DNA Library Preparation Kit	Illumina	FC-131-1024
SuperScript III First-Strand Synthesis System	Thermo Fisher Scientific	18080051
PrimeTime qPCR Assays	Integrated DNA Technologies	N/A
FastStart Universal SYBR Green Master (Rox)	Roche Molecular Systems	4913850001
MethoCult™ GF M3434	STEMCELL Technologies	3444
MethoCult™ GF M3534	STEMCELL Technologies	3534
MethoCult™ M3630	STEMCELL Technologies	3630
Deposited Data		
Raw and analyzed sequencing data	This paper	NCBI SRA database with number: PRJNA599415
Experimental Models: Cell Lines		
Cell: AGS Cell Line	Sigma-Aldrich	Strains:89090402
Cell: AGS-E Cell Line	Our lab (*J Biol Chem. 2004 Mar 5;279(10):8684-93*)	N/A
Experimental Models: Organisms/Strains		
Mouse: C57BL/6J	The Jackson Laboratory	Stock No: 000664

REAGENT or RESOURCE	SOURCE	IDENTIFIER
Mouse: R26-tdTomato	The Jackson Laboratory	Stock No: 007914
Mouse: GAS-KO	The Jackson Laboratory	Stock No: 031681
Mouse: Cck2r $^{-/-}$	The Jackson Laboratory	Stock No:006369
Mouse: Cck2r-CreERT	This paper	N/A
Mouse: C57BL/6J	The Jackson Laboratory	Stock No: 000664
Mouse: Eef1a1-LSL-Notch1(IC) mice	Dr. Kenneth Olive (Columbia University)	N/A
Mouse: LSL-Trp53R172H mice	Dr. Kenneth Olive (Columbia University)	N/A
Mouse: Apc $^{flox/flox}$ mice	the National Cancer Institute (NCI)	N/A
Mouse: Lgr5-DTR-GFP mice	Genentech	N/A
Mouse: Lgr5-GFP-IRES-CreERT2 mice	Dr. Hans Clevers	N/A
Software and Algorithms		
ImageJ version1.51h	N/A	http://imagej.net
Fiji version 2.0.0-rc54	N/A	http://imagej.net
FlowJo	FlowJo	https://www.flowjo.com
GraphPad Software	GraphPad Software	http://graphpad.com
Broad FireCloud computing system	N/A	https://software.broadinstitute.org/firecloud/
Picard Tools at Broad Institute	N/A	http://broadinstitute.github.io/picard/
Other		
Whole exome sequencing: Pair-end (PE) libraries were prepared and sequenced on the Illumina HiSeq instruments	Broad Institute, Columbia University Medical Center and Beijing Genomic Institute (BGI)	N/A